Temperature and strain dependence of fluorescence in praseodymium-doped silica optical fibre

A thesis submitted by

Bernhard Georg Koziol

for the degree of

Master of Science (Research)

Optical Technology Research Laboratory
School of Electrical Engineering
Victoria University

2004

Would our lives be improved if gold and uranium were as obscure and unimportant on Earth as praseodymium?

- Carl Sagan, Cosmos

Declaration

I, Bernhard Georg Koziol, declare that this thesis titled,

"Temperature and strain dependence of fluorescence in praseodymium-doped silica optical fibre"

is the result of work performed by the author and has not been submitted previously, in whole or part, in respect to any other academic award.

I also confirm that this thesis does not exceed 100,000 words.

Bernhard Koziol

Dated on the 17th day of August, 2004

Acknowledgments

This thesis could not have been completed without the help of many people. Firstly, I would like to thank Associate Professor Stephen Collins for allowing me to undertake my master's course at the Optical Technology Research Laboratory (OTRL) at Victoria University. I'd also like to extend my gratitude to both Stephen Collins and Associate Professor Greg Baxter, for their help, wisdom and continuing support over the candidature period.

I would also like to extend my gratitude to everyone in the post graduate office, and post-doctoral members of the Optical Technology Research Laboratory, who have helped me over the years, in helping out with the research and lowering my table tennis handicap (may the table-tennis table remain as a source of inspiration). Also, special thanks to both David Simpson and Claire Rollinson, for their helpfulness, humour, healthy competition and camaraderie during our university time together.

Also, I would like to extend my thanks to the technical staff in the physics department, especially Hayrettin Arisoy, Donald Ermel and Abdurrahman Kuzucu, who helped me overcome computer failure, and for machining specialised components, ordering optical equipment and finding equipment in the laboratory labyrinth.

I would like to thank more than ever my family for supporting and putting-up with me over the past six years. My parents, Gerhard and Barbara, for your support both emotionally and financially; I always look forward to arriving home after the long trip every night. Also, I would like to thank my siblings, Michael, Christine and Regina, for their support and understanding.

Finally, I would like to thank my friends outside of Victoria University especially the past, present and affiliated members of Monty Antioch who have helped me in many small but profound ways; encouraging me to keep going and not to lose sight of the bigger picture. Thankyou all once again!

Abstract

Temperature and strain measurement is an important requirement in many industrial processes. In areas where high electromagnetic fields, flammable environments or other adverse environments limit the use of electronic-based sensors, optical fibre-based sensors can be incorporated.

In this thesis, praseodymium (Pr^{3+}) -doped silica optical fibres were investigated for their temperature and strain properties using the fluorescence lifetime technique. These fibres had a Pr^{3+}-ion concentration of 700 ppm and 1000ppm, the latter of which was co-doped with Al^{+3} at a concentration of 4000 ppm.

The Pr^{3+} ion were excited with light from an argon-ion laser, centred at a wavelength of 488 nm. Two fluorescence wavelengths that emanated from the $^1D_2$ energy level were detected and measured, as the doped optical fibre was subject to temperatures between 20 and 700 °C, or was strained over a range from 0 to 1957 με.

Results from these measurements indicate that the temperature and strain sensitivity from these two fibres is comparable to that of other rare-earth-doped silica optical fibres. The fluorescence lifetime strain-dependence from the optical fibre with a Pr^{3+} concentration of 1000 ppm had a negative trend with increasing strain; this is contrary to other rare-earth-doped silica fibre strain sensitivities.

Contents

1 Introduction

1.1 Optical fibre properties

Optical fibres have been used extensively in the telecommunications industry from soon after their development. Since then, other fields in optical fibre technology have opened, including the medical, laser and sensing fields. Concurrent with this, there have been many improvements in manufacturing techniques for these devices.

Optical fibre sensors can be divided into two categories, *extrinsic* and *intrinsic*. Extrinsic optical fibre sensors use optical fibres to guide light to an exterior sensing material, or, to guide light to a detector that decodes information in the light signal that has travelled along the fibre. Extrinsic sensors can also be used for remote temperature sensing. Intrinsic sensors on the other hand use physical changes along the waveguide that affects some detectable property of the light (e.g. polarisation, phase or intensity). The benefits that optical fibres have over other established technologies include [1]:

- Immunity to electromagnetic (EM) interference
- Small size
- Light weight
- Electrical isolation
- High bandwidth
- Easily bonded to, or embedded in materials

Immunity to electromagnetic radiation enables the sensor to be used in areas that have high levels of electromagnetic radiation (eg. power stations, heavy industry). Electronic-based sensors would not be able to operate effectively in the same environment due to signal corruption from electromagnetic interference.

As optical fibres are inherently small (diameters of approximately 125 μm and lengths that can be as short as a several centimetres), they can be used in places where volume is an issue. Optical fibre sensors are also lightweight; this allows their use in systems where mass distribution is a critical factor (i.e. they don't "load" the structure).

Optical fibres are usually made from glass or from other electrically non-conductive materials, such as plastic, so they can be used safely in areas where high voltages exist. They have a high bandwidth; this enables optical fibre–based sensors to be wavelength multiplexed, allowing multiple sensors to be distributed along the fibre.

Optical fibres are easily bonded to a variety of surfaces that can be used to measure parameters such as temperature and strain along or through a test material. For this reason and their lightweight nature means that optical fibre based sensors are an attractive option in the aerospace industry.

1.2 Project aim

Optical fibre sensors doped with rare-earth ions have been investigated in detail over the years, as rare-earth ions are readily soluble in fibres and have long fluorescence lifetimes, thereby simplifying detection schemes.

Fluorescence lifetimes are inherently temperature sensitive, and investigations by many authors to measure how different rare-earth-doped fibres are affected by temperature have been conducted. There has also been some investigation to see how strain affects the fluorescence lifetime in some rare-earth-doped optical fibres.

This thesis investigates how the fluorescence lifetime from the $^1D_2$ energy level is influenced by temperature and strain in praseodymium-doped silica optical fibre. Results from these measurements will be compared to work on neodymium-, erbium- and ytterbium–doped optical fibre to assist in the physical understanding of how strain affects the fluorescence lifetime.

1.3 Summary of thesis content

This thesis is divided in a number of sections; each is briefly discussed. The use of temperature and strain sensors that are commonly used in industry, both optical and non-optical methods, will be shown in Chapter 2, with a greater emphasis on optical fibre-based methods. Chapter 3 will introduce optical fibres and the manufacture of

rare-earth-doped optical fibres. Properties of rare-earth ions and the effect of host materials on their optical properties will be discussed with particular attention paid to praseodymium-doped silica glass.

Chapter 4 will discuss fluorescence and non-radiative processes (phonon and cross-relaxation interactions), as well as models developed by researchers that describe temperature and strain effects on the fluorescence lifetime. Measurements of the fluorescence properties of praseodymium-doped optical fibres will also be reviewed.

Chapter 5 illustrates the optical arrangements for both temperature and strain fluorescence lifetime experiments used in this investigation; including a discussion on the apparatus that were necessary for this investigation. Chapter 6 will discuss the results from the experiments. Chapter 7 will compare the results from this project to those of other rare-earth–doped optical fibres (neodymium, erbium and ytterbium) that have been investigated by other authors.

Chapter 8 will provide concluding comments on the work described in this thesis and where future research may be undertaken.

2 Review of temperature and strain measurement systems

2.1 Chapter overview

The ability to measure strain and temperature accurately is paramount in many circumstances, from monitoring the structural integrity of buildings, dams and aircraft, to measuring temperature of furnaces, chemical or manufacturing processes.

There are a wide variety of temperature sensors available. Temperature can be measured by monitoring a changing physical parameter such as electrical resistance, volumetric expansion, vapour pressure, and spectral characteristics of the sensing material [2]. The earliest thermometer was designed by Galileo Galilei some time between 1592 and 1603 [3], known as a thermoscope. An air-filled bulb was attached to a pipe with the open end immersed in a coloured liquid. As temperature varied, air in the bulb either expanded or contracted, affecting the water level in the pipe.

The concept of the strain gauge was envisioned by Lord Kelvin in 1856 [4] when he noticed that resistance in an electrical conductor changed when stretched. However, it was not until the 1930s that strain gauges were widely used in industry.

The fundamental principal of strain gauges has not changed over the years; a material is deformed (eg. stretched) and a property (such as electrical resistance) is measured and compared to a calibration chart so the applied strain can be known.

2.2 Non-optical temperature and strain measurement systems

The following section explains the various systems used in non-optical based temperature and strain sensing. The simplest temperature sensor is the liquid-in-glass thermometer, and the foil gauge is the simplest strain sensor. Other forms of widely used temperature and strain sensors will be discussed briefly.

2.2.1 Temperature measurement systems

There are varieties of non-optical temperature measuring systems. These involve a physical change in the temperature-sensitive medium, such as volumetric distortion (thermometer), change in electronic properties such as resistance (thermistor), or the creation of small voltages (thermocouple). Some non-optical devices are summarised in table 2.1.

Table 2.1 *A sample of available non-optical temperature sensors, listing their details.*

Measurement Technique	Description	Temperature Range (°C)	Sensitivity	Advantages	Disadvantages	Ref.
Liquid in glass	Volumetric distortion of liquid against scale	-38 → +600 (Hg) -200 → +50 (Pentane)	25% of smallest increment	Low cost Ease of use	Fragile Parallax error Pressure effects Size	[5]
Thermocouple	Measuring the Seebeck voltage of dissimilar metals	0 → +760 (J-type) 0 → +1260 (K type)	55.9 μV/°C 40.7 μV/°C	Low cost Small size Reasonable uncertainty and stability	Weak signal Corruptible with EM radiation Non-linear output Requires amplification	[2]
Platinum resistance thermometers	Measuring the resistance change of platinum when applied to temperature environment	-259 → +750 †	0.4%/°C‡	Chemically inert Low uncertainty High resistivity	Strain sensitive Expensive	† [6] ‡ [5]
Thermistor	Resistance change in a semi-conducting material	-200 → +1000	-5%/°C	Low cost, high sensitivity Small size	Non-linearity Corruptible with EM radiation	[2]
Semi-conductor junction resistance thermometers	Thermal conductivity of diode/transistor junction is exploited.	-55 → +150	10 mV/°C	Simple circuitry Readily available Linearity	Self heating Non-linear at temperature extremes Can have high uncertainty	[7]

Thermocouples require two dissimilar metals that creates a small voltage that is dependent on the temperature. The voltage (Seebeck voltage) is proportional to the temperature at the junction of the two metals and requires amplification to be useful. Thermocouples are widely used in industry and research, as they are inexpensive and easy to obtain and are accurate, although they are not as resilient as platinum resistance thermometers and have less temperature range. Thermocouples create low voltages, for example at 100 °C the voltage is approximately 4 mV [2] and are therefore prone to EM interference. Thermocouples are also non-linear and their calibration can vary with contamination on the thermocouple materials [2]. In this project, temperature was measured with an Emtek (EMT-502) unit utilising a K-type thermocouple.

The majority of electronic-based temperature sensors also incorporate simple circuitry. However, complex circuitry can be incorporated to reduce the effects of resistance in the lead wires and to reduce noise from EM fields.

2.2.2 Strain measurement systems

Examples of common non-optical strain sensors are described, all of which require electronics to measure strain. Table 2.2 lists the various strain gauges that will be discussed in this chapter. The table includes their strain range, sensitivity, as well as an indication of their advantages and disadvantages. All of the strain sensors listed are sensitive to EM interference.

Table 2.2 *Summary of non-optical-based strain gauges.*

Measurement Technique	Maximum Strain (με)	Sensitivity	Advantages	Disadvantages	Ref.
Resistance strain gauge	25000	0.1% @ 4000 με 1% @ 10,000 με	Low cost Linear output Easy to install. Many configurations available	Temperature sensitive, at high temperatures Repeatability is difficult to achieve	[8]
Capacitance strain gauge	1500	0.018 pF/1000 με/m	Can be used in high temperature environments	Measurement leads create their own small capacitance	[4]
Semiconductor strain gauge	5000	± 1% @ 1000 με	Low hysteresis. Small size. High fatigue life	Made from photoelectric material (up to 2 or 3 με error), Non-linear output	[8]
Vibrating wire strain gauge	4000	± 10 με	Long lifetime (>15 years)	Restricted accuracy, Temperature dependent	[4]

Strain gauges were not used in this investigation. Instead, strain (ε) was determined by,

$$\varepsilon = \frac{\left(\frac{mg}{\pi r^2}\right)}{Y}, \tag{2.1}$$

where m is the mass of the weight, g is Earth's gravitational acceleration, r is the outer radius of the fibre, and Y is Young's modulus of the fibre's material. The pulley used to direct the fibre to hang vertically was approximated to have negligible friction.

2.3 Optical-based temperature and strain measurement systems

Optical methods of temperature sensing have the advantage over their electronic equivalents of being immune to EM interference. Each method has its own inherent advantages and disadvantages. As for electronic-based temperature sensors, no single sensor can be used to measure temperature in all situations.

Temperature and strain can be monitored at a point in space; these sensors are known as *point* temperature sensors, such as fibre Bragg gratings or fluorescence lifetime-based temperature sensors. Alternatively, they can be used to monitor temperature and strain over a given distance; these are known as *distributed* temperature sensors, an example of which is a Brillouin scattering-based sensor.

Optical-based measurement can use optics (eg. lens) to gather light from the target object by line of sight; otherwise, optical fibres can be used to redirect light to detectors. Optical fibres have a core and cladding region that allows light to be guided down the length of the fibre's core, caused by a difference in core and cladding refractive indices, namely n_1 and n_2 respectively as shown in figure 2.1. The core diameter of single mode optical fibres is about 8μm, increasing the core diameter can support multiple modes of light along the fibre.

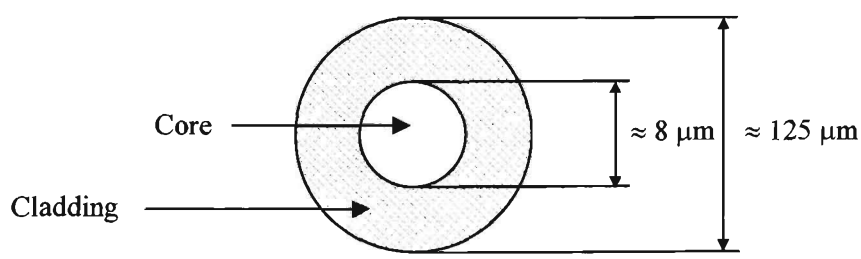

Figure 2.1 *Cross section of a typical optical fibre.*

The following table (2.3) is a sample of different techniques for optical based thermometry. Although the selected systems are limited to intrinsic designs, some of these systems can be modified to be extrinsic in design as well.

Table 2.3 *A sample of optical-based temperature measurement systems.*

Type	Temperature Range (°C) (Accuracy)	Sensitivity	Advantages	Disadvantages	Ref.
Absorption	-20 →350 -50 → 100	10^{-3}/°C 0.2%/°C	Simple optical arrangement Linear response	Limited range (semiconductor material) Difficult to bond to optical fibres	[9] [10]
Blackbody	400 → 1200 (± 10^{-2} at high temperature)		Remote sensing Fast acquisition time	Clear optical path required Not suitable for low temperature	[11] [2]
Brillouin scattering	25 → 60 (± 0.5) 20 → 80 (± 1)	1.36 MHz/°C	Long range distributed sensing Good spatial resolution	Strain sensitive Complex optical arrangement	[12] [13]
Fibre Bragg Grating	25 → 800 †	10 pm/°C (@ 1300 nm) ‡ (@ 1500 nm) *	Simple optical arrangement Good accuracy and sensitivity	Strain sensitive Expensive FBG disappear	† [14] ‡ [15] * [16]
Fluorescence Intensity Ratio	-50 → 500 (± 3.4) †	0.06 /°C ‡	Strain independent Good accuracy and sensitivity	Insensitive at low temperature Expensive	† [17] ‡ [18] [19]
Fluorescence Lifetime	0 → 850 (±5)	(9.7 ± 3.8) × 10^{-5} %/°C	Wide temperature range Ease of measurement	Strain-temperature cross- sensitivity Concentration quenching	[20]
Interferometry	20 → 800 (± 0.025) 20 → 800 (± 0.013)		Many configurations possible: Sagnac Loop † Mach-Zehnder ‡ Fabry-Perot * Easy to build Very accurate	Strain and polarisation sensitive Fibres need to be pre-annealed	† [21] ‡ [22] * [23] [24]
Raman Scattering	23 → 59 (± 4)	11 mV/nW	Distributed sensor (10 km) Good spatial accuracy (10 m)	Detector bandwidth limitation Peak power limitation	[25]

2.3.1 Optical-based temperature systems

2.3.1.1 Absorption

The amount of light that is absorbed by materials such as rare earths, or semiconductors is proportional to the temperature of the material. Barmenkov [9] used a CdSe crystal illuminated with a 630 nm LED. The 630 nm light was split into two paths; one being a reference, the other beam was shone through the crystal and detected. The ratio of both intensities was measured.

Using a similar scheme, Farries *et al.* [10] measured the change in the absorption spectrum of Nd^{3+}-doped fibre. The simple design and linear relationship of temperature and ratio between the reference light source and absorbed light make this type of sensing advantageous. However, the semiconductor material used by Barmenkov *et al.* [9] is difficult to incorporate into existing fibre networks and has a limited temperature range.

2.3.1.2 Blackbody measurements

Bodies will emit radiation due to their thermal energy. The spectrum of radiation emitted is not uniform; instead, the spectral peak shifts to shorter wavelengths as the energy of the body increases as described by Planck's Law.

Optical fibres can be used to sense blackbody radiation intrinsically, by use of a quartz rod that acts as a blackbody source when exposed to high temperatures. Quartz is often used because of its availability, relatively low attenuation in the required optical frequency domain and a relatively high softening point ($\approx$ 1200°C) [11].

The range of temperature measurements is determined by two factors, the softening point of the blackbody material at the high end of the range, and the sensitivity of the detector at low intensities, at the lower temperature range.

The advantages of utilising blackbody temperature sensing include remote temperature sensing of potentially dangerous environments and quick response time. However, false temperature measurements can be caused by the intensity of the signal from the heat source being altered by effects such as surface emissivity and

reflections, and fluorescence, absorption, scattering and the size of objects such as air molecules that are between the signal and detector [2].

The detection scheme calculates the temperature from the blackbody spectrum by either integrating the area under the spectrum or by the use of Planck's Law, if the maximum intensity wavelength is known.

2.3.1.3 Brillouin scattering

Distributed Brillouin scattering-based sensors use the interaction of two counter propagating light beams along an optical fibre core. One beam, the pump, produces acoustic waves along the core of the fibre; these waves can be likened to changes in refractive index. The other beam, the probe, interacts with these refractive index changes, and is Bragg reflected. This reflected light is frequency down-shifted by

$$\nu_B = \frac{2nV_a}{\lambda}, \tag{2.2}$$

where, ν_B is the frequency shift of the reflected probe. The refractive index of the fibre core is n, the velocity of the acoustic waves is V_a, and the probe's wavelength is denoted by λ. Both the refractive index and the acoustic velocity are temperature and strain dependent.

Brillouin scattering can provide distributed temperature measurements over distances of several kilometres. The configuration used by Boa *et al.* [13] had two laser sources, but the required access to both ends of the fibre, limits the effectiveness for remote sensing. Niklès *et al.* [12] demonstrated a simple way to measure Brillouin-based temperature sensing using a single light source that requires only one end of the fibre accessible. Polarisation maintaining fibre must be used to maximise the Brillouin signal. Launching the acoustic waves into the optical fibres is difficult and may be a limitation in future systems [1].

2.3.1.4 Fibre Bragg Gratings

Fibre Bragg gratings (FBGs) are periodical changes in the refractive index along the fibre core that can be considered an internal mirror that reflects at a particular wavelength. Equation 2.3 shows the relationship between the reflected wavelength λ_B, the refractive index of the fibre's core n, and the periodicity, Λ, of the grating.

$$\lambda_B = 2n\Lambda \tag{2.3}$$

Figure 2.2 is a simplified depiction of the input light spectrum and subsequent output spectra, both reflected and transmitted, of a fibre Bragg grating.

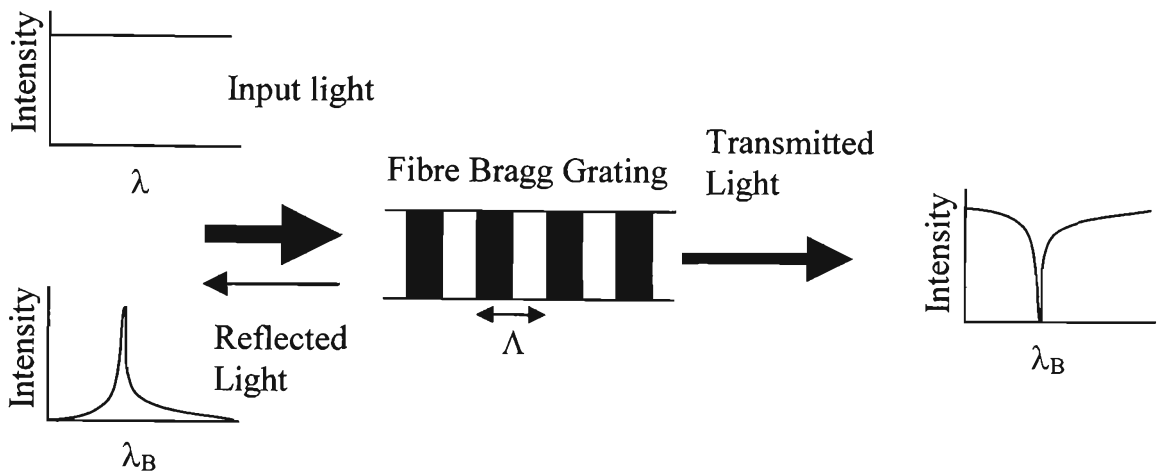

Figure 2.2 *A fibre Bragg grating reflects a narrow wavelength from a broad wavelength source. The reflection spectrum shows a peak at the reflected wavelength, whilst the transmission spectrum shows a dip where the Bragg wavelength lies.*

FBGs are created directly into the optical fibre core; the small changes in refractive index are produced by ultraviolet illumination. They are inherently temperature sensitive due to thermal expansion of the optical fibre, which increases the periodicity of the gratings, causing a shift in the reflected wavelength.

FBGs have the advantages that temperature is easily measured by monitoring the wavelength shift of the reflected wavelength, and can measure temperature with good accuracy and sensitivity. Recently, investigations by Trpkovski *et al.* [14] demonstrated that FBGs that were subject to high temperature, lost their reflectivity and later recovered the reflectivity to about 35% of its initial reflectance. After

annealing, the temperature stability of the FBG was found to be reliable for temperature sensing up to 800 °C.

2.3.1.5 Fluorescence intensity ratio

The fluorescence intensity ratio (FIR) technique takes advantage of fluorescence intensities from two closely separated energy levels that have been excited by a suitable pump source. The relative populations, and hence the emission intensities from these levels, is dependent upon temperature, due to a Boltzmann distribution. Figure 2.3 shows a typical energy diagram for fluorescence intensity ratio schemes.

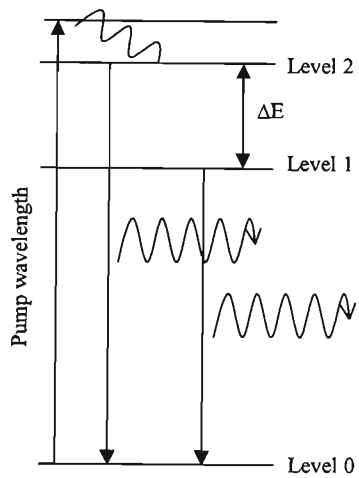

Figure 2.3 *A schematic diagram illustrating the optical processes for FIR-based thermometry. The thermalised levels (1 and 2) are separated by an energy gap, ΔE.*

FIR thermometry has been investigated comprehensively in rare-earth-doped fibres by Wade *et al.* [17] who measured the characteristics for praseodymium, neodymium, samarium, europium, dysprosium, erbium and ytterbium –doped fibres in a wide range of host materials. Temperature can be measured by integrating the area under two specific peaks of the fluorescence spectrum, and forming their ratio.

One of the most important features of FIR–based temperature sensing is that it is effectively strain independent [19]. This sensing scheme also provides a compact sensor with good sensitivity, temperature range and accuracy. For example, Nd^{3+}-doped silica fibre has been characterised for temperatures ranging from -50 to 500 °C with an accuracy of ±3.4 °C [17]. However, the required optical apparatus can become expensive and a high power pump laser is required for good signal-to-noise ratio.

2.3.1.6 Fluorescence lifetime measurements

Fluorescence lifetime (FL)-based thermometry measures the time that atoms take to decay into a lower state after being excited by an appropriate wavelength. The time taken for excited atoms to decay to lower states is temperature dependent. Various materials have been used by various authors; these include rare earths (praseodymium, neodymium, erbium, ytterbium) in many host materials, and Cr^{3+}-doped material such as ruby or alexandrite. These optically active media offer energy levels that have long lifetimes thereby simplifying detection schemes. In order to measure fluorescence lifetimes, a pulsed pump source is required to put the atom into an excited state, where decay from the excited level takes place, either radiatively, non-radiatively or both.

The advantages of FL-based sensing include small sensor, simple optical arrangement and fluorescence lifetime is easily measurable. Disadvantages include strain-temperature cross-sensitivity (-2.8×10^{-3} °C/με) for 990 ppm Nd^{3+}-doped fibre [26]), concentration quenching; where clusters of rare-earth-dopants alter the natural fluorescence lifetime through ion-ion interactions, thermal quenching; phonon emission reducing the fluorescence lifetime (occurs at temperatures above 400 °C for Yb^{3+}-doped silica fibre).

Temperature ranges that FL can be accurately measured range from 0 to 850 °C with a temperature error of ±5 °C for a Er/Yb doped silica fibre [20]. For higher temperature measurements, the fibre needs to be annealed before use in these temperatures in order to minimise hysteresis effects in the measured fluorescence lifetimes.

2.3.1.7 Interferometry

Interferometers work by measuring the phase change between two optical paths. One path acts as the reference; it is temperature stabilised and spatially static. The other path is the sensing path; it is where the measurand is sensed. The two light signals are superimposed and the phase difference is measured. In–fibre interferometer–based temperature sensors have been demonstrated using both single wavelength and white light sources. There are many configurations that may be used, such as Sagnac loop [21], Fabry-Perot and Mach-Zehnder [22].

Low coherence interferometers have the following advantages: wide temperature range (20 to 800 °C), high resolution, in the order of 0.025°C, based on a 1 mm Fabry-Perot interferometer [23].

White light interferometry has the advantage of high-resolution temperature sensing (0.013 °C) across a temperature range from 20 to 800 °C [24]. The high resolution has been attributed to the use of two interferometers to determine the position of the scanning mirror. White light interferometers also have the additional advantage that they do not have the need to be calibrated when installed, unlike single wavelength interferometers, and they can be multiplexed.

In-fibre interferometers have the following disadvantages, strain–temperature cross–sensitivity, polarisation controllers are required to enhance fringe contrast, and the sensing fibre needs to be annealed to minimise reading error. Two interferometers are required when using white light interferometry.

2.3.1.8 Raman scattering

Optical fibre distributed temperature sensors enable the temperature profile along a length of fibre to be monitored continuously. These sensors use optical time domain reflectometry (OTDR) whereby a pulse of light that is transmitted down the fibre and the backscattered light, which is within the numerical aperture of the fibre, is detected. The time between sending the light and detecting the backscattered signal provides a measure of the distance along the fibre, whilst the intensity of the Raman backscattered light provides information on temperature. In order to predict temperature changes the Raman signal must be referenced to the temperature–

independent Rayleigh signal which must be measured with the same spatial resolution. Advantages of Raman-based temperature sensing include: only one end of the fibre is used, temperature readings can be taken over many kilometres of fibre, and the resolution of temperature readings is ± 4 °C, with a spatial resolution of 10 m [25].

Raman distributed temperature sensing can cover distances of 10 km and can be incorporated to monitor existing telecommunication fibres at 1.65 μm, as demonstrated by Kee *et al.* [25]. This system provides good temperature and spatial accuracy, 4 °C and 10 m, respectively. Raman-based temperature sensing is restricted to non-amplified communication links.

2.3.2 Optical-based strain systems

As mentioned in the section 2.3.1, most of the optical-based temperature sensors are also inherently strain sensitive. When the strain properties can be exploited successfully, that is, temperature compensated or used in a steady temperature environment, then these strain sensors have the same flexibility as other optical fibre-based systems. Table 2.4 lists some optical-based strain sensors.

Table 2.4 *A selection of optical fibre-based strain sensing schemes.*

Sensor Type	Strain Range (με) (Accuracy)	Sensitivity	Advantages	Disadvantages	Ref.
Brillouin scattering	± 2000 (±50)		Distributed sensor Good accuracy	Complex optical arrangement Strain –temperature cross-sensitive	[27]
Fibre Bragg grating	0 → 2000 (±0.426) †	1pm/με @ 1300 nm ‡	Simple optical arrangement Quasi-distributed strain sensor	Strain-temperature cross-sensitive	† [28] ‡ [15]
Fluorescence lifetime	0 → 2000	5×10^{-5} %/με	Simple optical arrangement Ease of measurement	Strain-temperature cross-sensitivite	[1]
Interferometry	± 6000		Simple optical arrangement Can be multiplexed	Polarisation -maintaining fibre required. Strain-temperature cross-sensitive	[29]

2.3.2.1 Brillouin scattering

Brillouin scattering can also be used to measure strain along an optical fibre in addition to temperature as already discussed in section 2.3.1.3. In an investigation by DeMerchant *et al.* used a 2.4 m long sensor that had a resolution of 0.4 m and an accuracy of ±50 με over a strain range of ±2000 με was created. [27]. Brillouin-based strain sensing can take multiple strain measurements along the fibre, over long distances. [30].

2.3.2.2 Interferometry techniques

Interferometers are also strain sensitive, this is due to path lengths changing in relation to strain, thus affecting phase changes when the signal and reference signals are superimposed. Based on a white light Michelson interferometer, strains up to 6000 με were measured until the epoxy de-bonded the fibre optic extensometer [29].

2.3.2.3 Fibre Bragg gratings

The periodicity of the grating is changed due to the applied strain. Typical strain sensitivities are in the order of 1 pm/με at 1300 nm illumination as determined with the use of an optical spectrum analyser [15]. The strain range of FBGs is up to the breaking point of the fibre, about 2000 με.

Allsop *et al.* [28] measured strain using a FBG with a precision of ±0.43 με, which is similar to the precision of the Fabry-Perot interferometer. This was achieved by creating a Michelson-type interferometer as the sensor. The first and second harmonics were then interrogated for data about strain. This system, has the advantage of not requiring an OSA and is relatively inexpensive to implement However this system is also affected by temperature.

2.3.2.4 Fluorescence lifetime measurement

The strain sensitivity for FL-based strain measurement is in the order of 5×10^{-5} %/με, with a maximum strain range of approximately 2000 με [26]. The temperature dependence on FL can create erroneous results when taking strain readings; therefore, the temperature of the strain sensing fibre must be taken into consideration.

2.4 Simultaneous temperature and strain measurement systems

Temperature and strain cross sensitivity is common amongst most optical fibre sensing schemes, and it is through this that researchers have been able to measure both temperature and strain simultaneously. Thus it was realised that different methods of optical-based temperature and strain measurement systems have dissimilar temperature and strain coefficients therefore both the temperature and strain can be determined.

Examples of simultaneous temperature and strain measurement systems include fluorescence lifetime – fibre Bragg grating [31], fluorescence intensity ratio- fibre Bragg grating [32], Brillouin scattering [33], dual fibre Bragg grating [34], amongst others.

2.4.1 Fluorescence lifetime – fibre Bragg grating

Dual temperature-strain measurements can be measured by incorporating Er^{3+} or Er^{3+}/Yb^{3+}-doped fibres in series with a FBG as described by Forsyth *et al.* [31].

The fluorescence from the rare-earth-doped fibre is used to illuminate the grating, which has a central wavelength in the 1550 nm region. This central wavelength shifted when strain or temperature change were applied to the fibre. Forsyth's system had a strain and temperature resolution of 7 με and 0.8 °C, up to 1860 με and 120 °C, respectively.

2.4.2 Fluorescence intensity ratio – fibre Bragg grating

Simultaneous measurement of temperature and strain can be achieved by using both the FIR and a FBG. FIR is effectively strain independent (section 2.3.1.5) and can therefore be used as a reference for temperature, whilst the FBG can be used to determine the strain once the temperature is known.

A system investigated by Trpkovski *et al.* [32] used a short length of Er^{3+}-doped silica fibre spliced to another fibre that had a FBG centred near 1535 nm, to be illuminated by fluorescence from the Er^{3+} ions. Using a matrix method provided standard deviations of 2.2 °C and 20.6 με, while a quadratic fit for temperature and a linear strain fit resulted in 1.0 °C and 22.9 με over a temperature and strain range of 18 – 150 °C and 350 – 2534 με, respectively.

2.4.3 Pairs of fibre Bragg gratings

FBGs, as mentioned earlier (section 2.3.1.4), have a strain-temperature cross-sensitivity issue. There are several ways to create a simultaneous temperature-strain sensor. One method for temperature-strain discrimination is to place two FBGs of different central wavelengths in series along a fibre. The temperature coefficients remain similar, but the strain coefficients are different, this can be exploited to determine both temperature and strain along fibre. An investigation by James *et al.* [34] was able to measure temperature and strain from two FBGs that were written on two different fibres that were fusion spliced between these FBGs. These measurements were over a temperature range of 20 to 160 °C and a strain range from 0 to 2500 με with maximum uncertainties of ± 1 °C and ±17 με.

2.4.4 Brillouin scattering

Brillouin-based systems can also be used to measure temperature and strain simultaneously for distributed sensing applications. Lee *et al.* [33] investigated a system using this method along a 3682 m single mode optical fibre. Lee was able to measure temperature and strain to a resolution of 5 °C and 60 με, respectively, with a spatial resolution of 2 m.

2.5 Conclusion

There is a wide range of temperature and strain sensors that are available, or under development, to improve current measurement systems. Electronic-based systems are inexpensive and readily available, and able to meet the requirements of many situations. Unfortunately electronic-based sensors are susceptible to EM interference; this can cause measurements to become corrupted or may swamp the signal with noise. Although liquid-in-glass thermometers are not susceptible to EM interference, their bulk is their primary limiting factor.

Optical-based temperature and strain sensors allow for measurements in areas of high EM fields. These measurement systems are available on the market, but as they are generally more expensive than their electronic counterparts, it is often stated that optical fibres sensors are suitable for certain niche markets. They are also more expensive than their electronic counterparts since they may require a light source (laser or high power LED) at uncommon wavelengths, or customised optical fibre (e.g. polarising-maintaining fibre).

There is a wide variety of optical-based temperature and strain sensing devices currently available, or in development, including dedicated temperature or strain sensors, or strain-temperature dual sensors that are becoming more flexible to suit a variety of applications.

No single sensor that is suitable for all situations. Therefore careful consideration must be used to ensure that the most suitable sensor is used for the required measurement.

3 Rare-earth-doped materials

3.1 Chapter overview

In this chapter, the properties of silica optical fibre includes a brief description illustrating how rare-earth ions are infused in optical fibres using the modified chemical vapour deposition (MCVD) technique. Optical applications of praseodymium-doped optical fibres, which include fibre lasers, optical amplifiers and fibre-based sensors, will be presented.

3.2 Silica-based optical fibre

Silica-based optical fibres are used extensively in optical telecommunications as the medium through which light travels along to pass information between two parties. Optical fibres are usually comprised of two sections, the core and the cladding as shown in figure 3.1. Normally, these are comprised of vitreous silica (SiO_2), and with the addition of germanium oxide (GeO_2), boron oxide (B_2O_3), or phosphorous oxide (P_2O_5) to increase the refractive index of the core (n_1); this causes light in the core to be effectively trapped, by total internal reflection, as n_1 is greater than n_2.

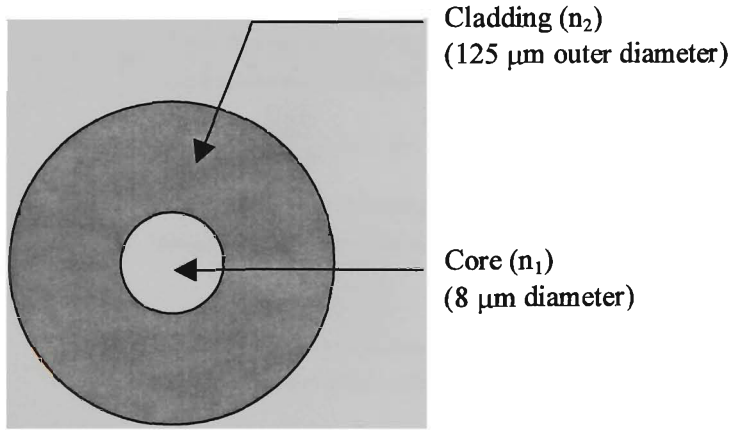

Figure 3.1 *A cross section diagram of an optical fibre. The two main regions are the cladding, which has a lower refractive index than the core. Core and cladding diameters shown, are those from the fibre used in this research.*

Silica glass optical fibre can be used in a wide temperature range, this is attributed to its high glass transition temperature (1175 °C); it also has a low specific heat capacity

(0.749 $Jg^{-1}°C^{-1}$) and low thermal conductivity (1.38 W $m^{-1}°C^{-1}$) [35]. These properties make silica glass fibres appropriate for temperature sensing, as they do not act as a heat sink. Their mechanical properties include a density of 2.2 g cm^{-3}, and a Young's modulus of 70 GPa [35]. However, the theoretical strength of silica-based optical fibre is greater than the actual strength for the following reasons. Firstly, due to manufacturing and handling tolerances, the outer surface of the optical fibre is prone to scratches and other flaws that decrease the overall strength of the fibre by amplifying stress at these points. Flawless glass can also have less than the expected theoretical strength due to water, or water vapour contamination, which over time further weakens the fibre.

The praseodymium-doped silica optical fibres used in this thesis were manufactured at the *Laboratorie de Physique de la Materière Condensé, Université de Nice*, France, using the modified chemical vapour deposition (MCVD) technique.

The MCVD manufacturing technique enables long lengths of optical fibres with low concentrations of rare-earth ions to be created; low concentrations of rare-earth ions in long fibres take advantage of long interaction lengths and low losses that are inherent in telecommunications-grade fibre. The MCVD technique, shown in figure 3.2 (a–d), uses glass forming gases that are introduced into the deposition tube.

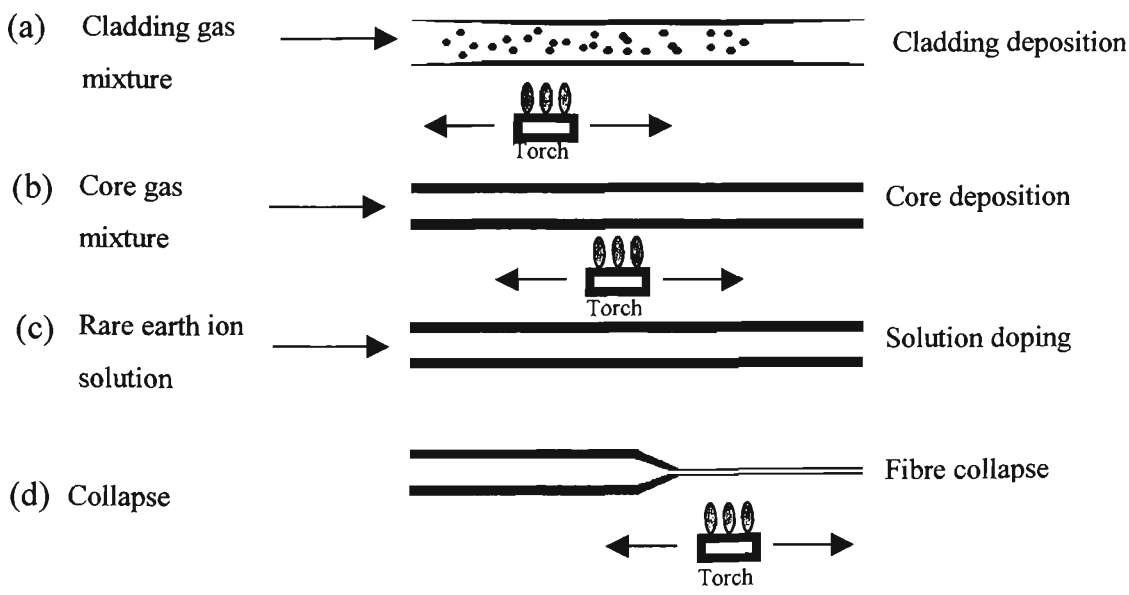

Figure 3.2 *MCVD diagram illustrating the main processes in the production of optical fibres that are doped with rare-earth ions.*

The deposition tube is rotated above a high temperature burner that sweeps along the tube's length. After several layers of cladding vapour, (figure 3.2(a)), have condensed on the inner walls of the tube, the vapour composition is changed, by addition of oxides such as B_2O_3, GeO_2 and P_2O_5, to start forming the core (figure 3.2(b)). After several layers of core forming material has condensed on the inner surface of the tube, the rare-earth ion(s) are introduced (figure 3.2(c)), either by soaking the inside of the preform with a rare-earth-doped solution, or by lacing the vapour with rare-earth ions. The rare-earth ions are allowed to impregnate itself into the core region. Afterwards, the tube is thoroughly dried by brushing a high temperature flame along the length of the tube. By increasing the temperature of the flame, the tube collapses into a preform (figure 3.2(d)). The preform is later heated in a tower, allowing a fibre to be drawn out and coated with a protective sheath to protect the fibre from both water penetration and general handling.

3.3 Rare-earth elements

The rare-earth elements have had a long history in the fields of optical and magnetic science. They can be found on the periodic table of elements in the lanthanide and actinide series, as shown in figure 3.3. These two groups are very different from each other; the actinide elements are all radioactive and over half of them are synthetic, due to nuclear instability.

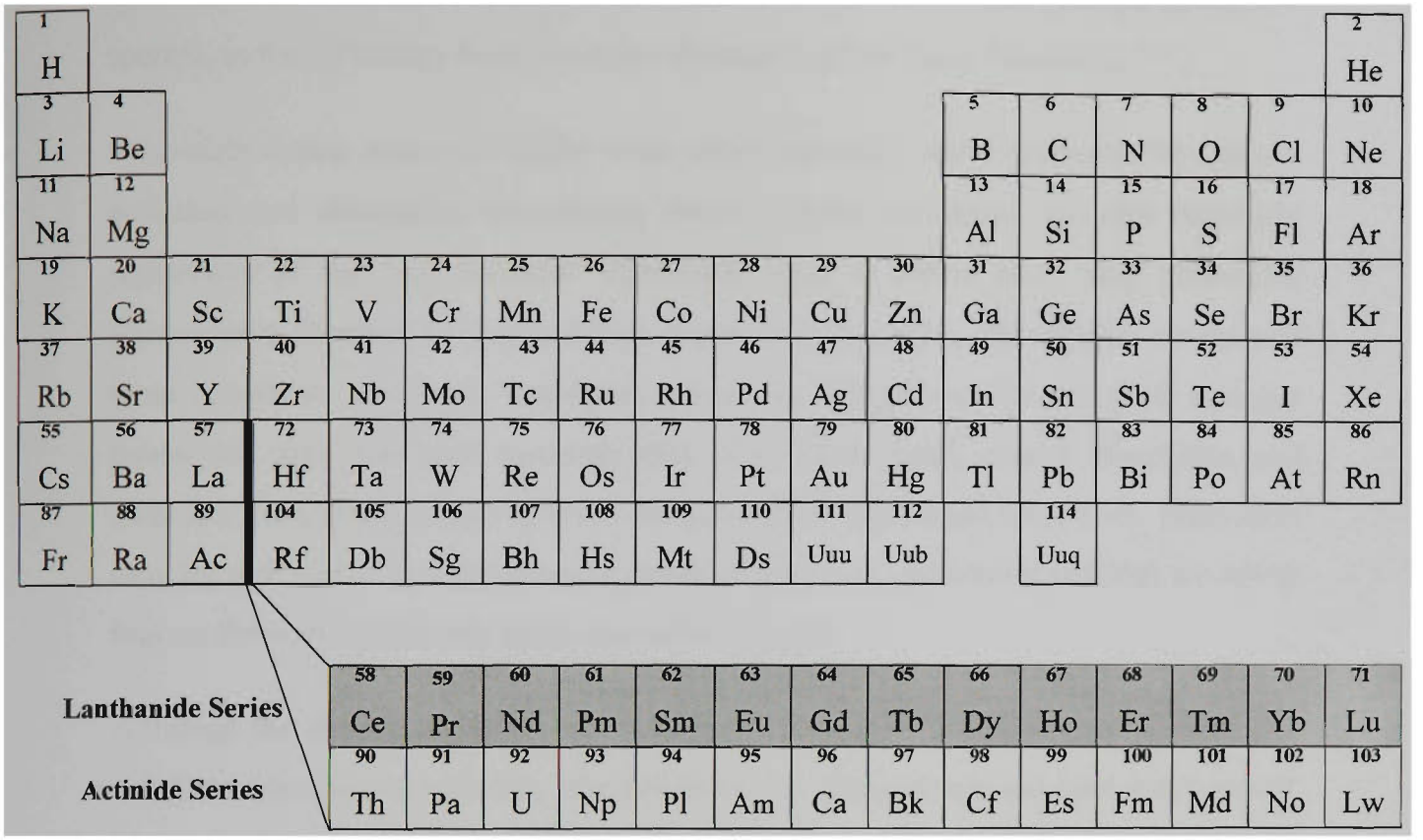

Figure 3.3 *The periodic table of the elements including the atomic number of the elements; the Lanthanide series is highlighted.*

The lanthanide series on the other hand are all found naturally, except for promethium, which has a short lifetime (<20 years) and can only be prepared artificially. The lanthanide series (which will be now referred as rare-earth), have the same core electron configuration as xenon (Xe). Atomic mass increases through the filling of the 4f orbital, beginning with cerium (Ce) and ending with lutetium (Lu). The 4f shell is effectively shielded from local fields in the host material as the 5s and 5p electron shells are full [36].

In condensed matter, rare earths have a trivalent (3+) level of ionisation; this is the most stable configuration for optical devices. Ionisation preferentially removes the 5s and 5d electrons, leaving the same electronic configuration of Xe with additional 4f electrons, depending on which rare-earth ion is used. Figure 3.4 shows the energy levels that are allowed from interactions of the 4f shell electrons. The vertical scale is energy in terms of cm^{-1} on a $\times 1000$ scale.

Transitions from the 4f electrons are responsible for the visible and infrared emissions from the rare earth ions. Only Ce^{3+} and praseodymium (Pr^{3+}) can produce strong UV spectra, as the 5d energy level lies close enough to allow these transitions [37].

Rare-earth-doped materials differ from other optically active materials by narrow emission and absorption wavelength ranges; these transitions are also relatively insensitive to the host material. Rare-earth ions in solids have long metastable fluorescence lifetimes (>1μs) and high quantum efficiencies, although the strength of these transitions are weak. Transition metals, in comparison, have a much stronger interaction with the host material; they also have broad, strong absorption and emission wavelength ranges as these are assisted by vibrational transitions. Rare-earth ions are well suited for optical applications as their non-radiative transitions are not as high as those from optically active transition metals.

Although the energy levels for rare-earth ions shown in figure 3.4 are measured in anhydrous lanthanum chloride, the positions for these levels are host independent. However the energy width of these energy levels are host dependent, as well as the radiative and non-radiative rates (see Chapter 4). Rare-earth-doped materials have been used to produce lasers operating over a wide range of wavelengths in the UV, visible, and the near-infrared bands, and optical amplification for both 1.3 and 1.5 μm telecommunications windows [37]. As discussed in Chapter 2 they also find applications in temperature and strain sensing.

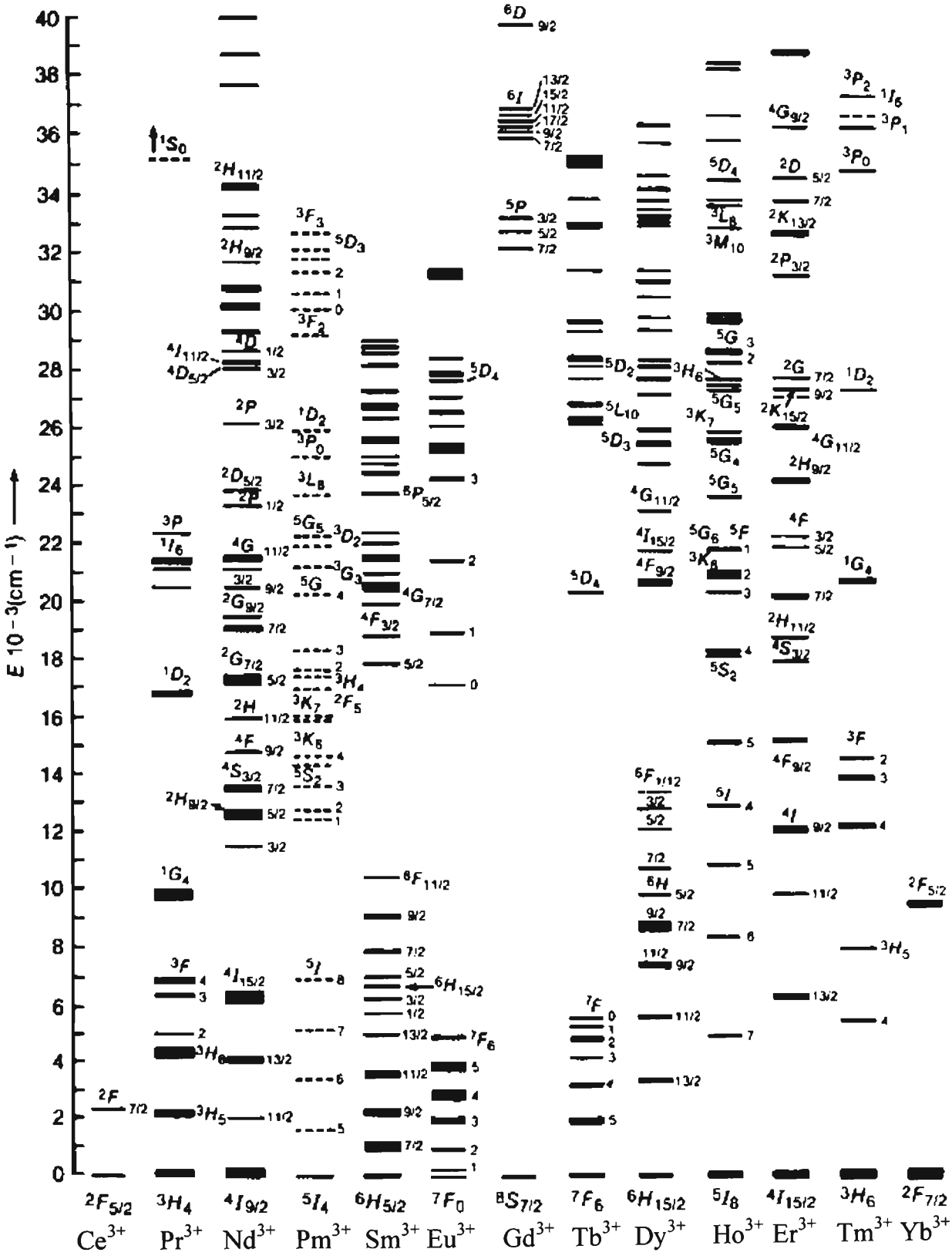

Figure 3.4 *Stark manifolds for trivalent rare-earth ions in anhydrous $LaCl_3$ [38].*

3.4 Praseodymium ion

Triply ionised Pr (Pr^{3+}) hosts several metastable energy levels, namely $^3P_0$, $^1D_2$ and $^1G_4$ (figure 3.4). These levels can be directly populated using 488, 590 and 980 nm illumination respectively, from the ground state as shown in the absorption spectrum in figure 3.5.

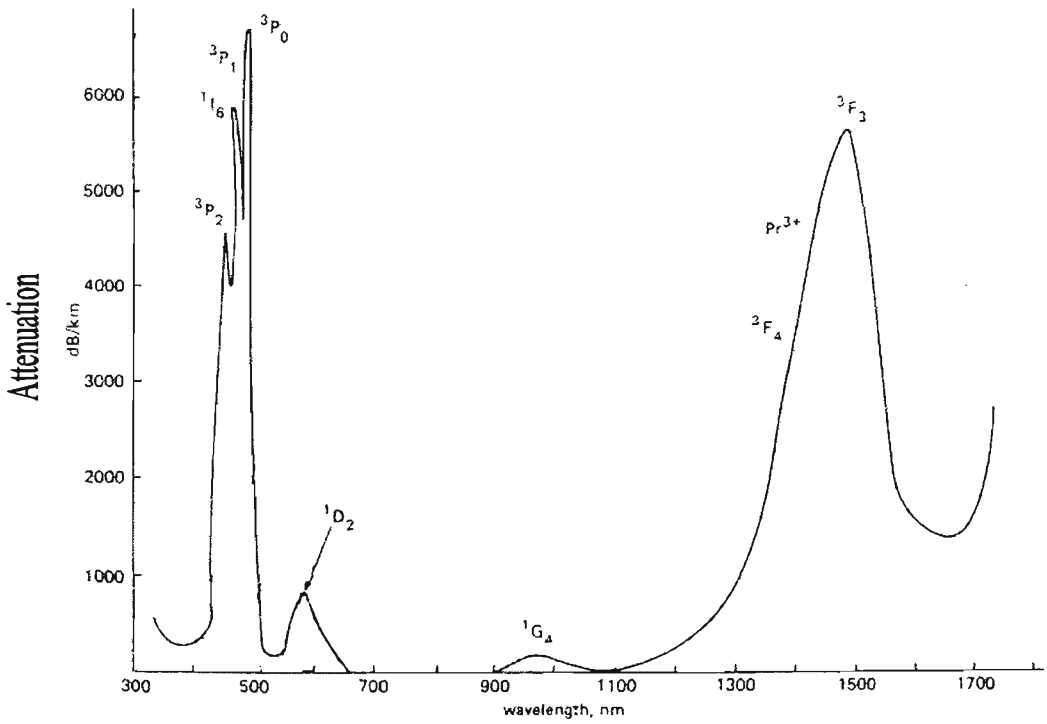

Figure 3.5 *Absorption spectrum of Pr^{3+}-doped silica fibre, the three metastable manifolds are clearly visible [after, [39], this reproduced diagram includes faults present in the original article].*

In the above figure, the ^3P triplet can be resolved in silica fibre, covering a wavelength range from 460 to 490 nm with the highest absorption peak accessible at a wavelength of 488 nm from an argon-ion laser. The $^1D_2$ energy level absorbs wavelengths near 590 nm, although not as strongly as the levels in the ^3P triplet.

A fluorescence spectrum (for 488 nm illumination) is shown in figure 3.6. Percival *et al.* [40] suggested that the majority of fluorescence peaks in Pr^{3+}-doped silica fibres are emitted from the $^1D_2$ energy level. This was determined by illuminating the Pr^{3+}-doped silica optical fibre with wavelengths of 590 and 488 nm, which recorded a fluorescence lifetime of 120 μs in either case.

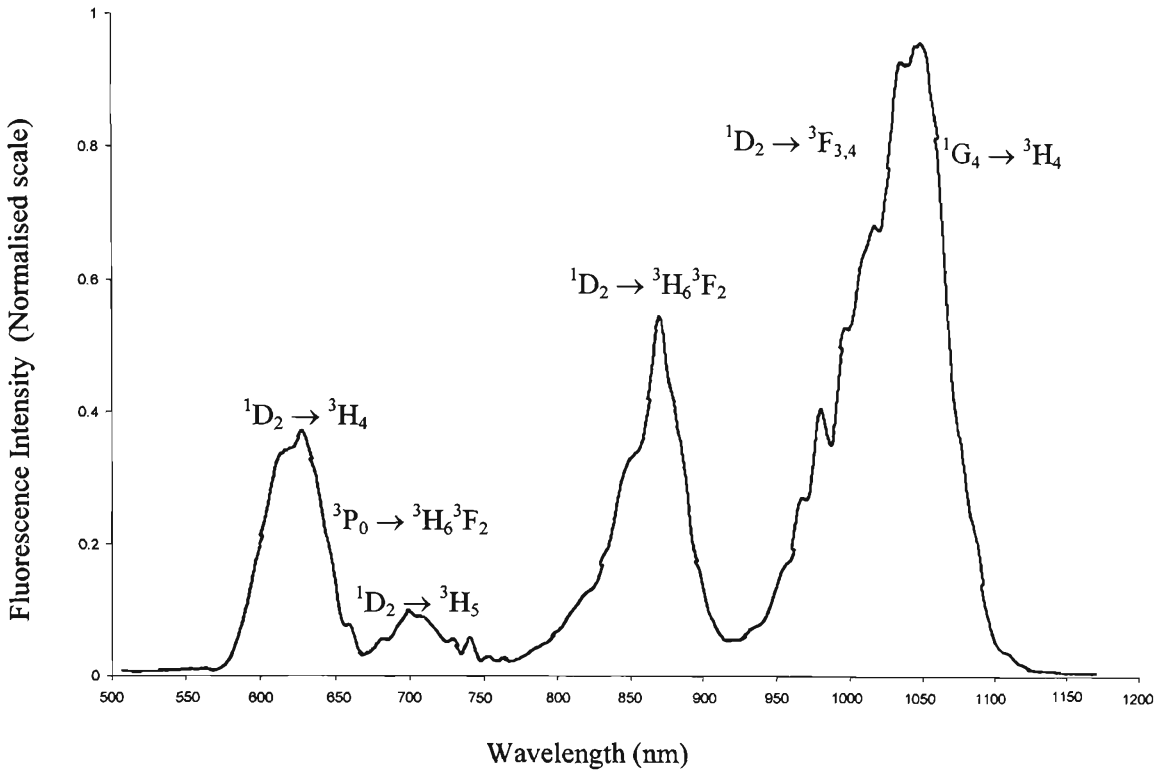

Figure 3.6 *Fluorescence spectra of Pr^{3+}-doped optical fibre. The spectrum was measured by the author of this thesis and the transitions are those assigned by Percival [40], showing that the majority of fluorescence peaks emanate from the $^1D_2$ energy level. Imperfections in this spectrum were caused by scanning errors within the optical spectrum analyser (Ando AQ 6310B).*

The above figure similar to the one shown in Percival *et al.*'s [40] investigation indicates that the majority of fluorescence peaks arise from the $^1D_2$ energy level,. This suggests that the $^1D_2$ energy level has the most efficient fluorescence properties from the three metastable states in a silica host.

Fibre lasers have been created using Pr^{3+}-doped silica; the wavelengths that have been found to lase (888, 1080 nm) originate from the $^1D_2$ energy level ($^3P_0$ and $^1G_4$ energy levels fluoresce very weakly in silica hosts) and are usually pumped at a wavelength of 590 nm. Pumping at a wavelength of 488 nm can also be used although the lasing threshold is higher [40]. Pr^{3+}-doped fluorozirconate glass (a glass that has a high heavy metal content) has more radiative transitions than silica glass and can therefore host more laser wavelengths. These occur at 610, 995, 715, 885 and 910 nm, and arise solely from the $^3P_0$ energy level [41]. Pr^{3+}-doped fluorozirconate glass can also be populated at the $^1D_2$ energy level. This requires a laser that has an output wavelength close to 590 nm.

Another application for Pr^{3+}-doped fibre is optical amplification at 1.3 μm. Initially Nd^{3+}-doped fibre using the $^4F_{5/2} \rightarrow {}^4I_{13/2}$ transition was thought to be the best transition [42]. However, excited state absorption at the $^4F_{5/2}$ energy level limited the efficiency for amplification and exotic (i.e. not silica-based) glasses are required for efficient amplification. Pr^{3+}-doped fluorozirconate fibre was found to be a better candidate for 1.3 μm amplification and is now commercially available [43], and is currently under further development to handle greater data rates and more channels [44]. The pump wavelength for these amplifiers is about 980 nm which is readily available. Amplification at 1.3 μm in Pr^{3+}-doped fibres has also been investigated in multi-component glasses such as: mixed halide (cadmium fluoride) [45], Cs:Ga:S:Cl [46] and tellurite [47] optical fibres. These fibres had good results, although their drawback are their mechanical properties, which are not as good as fluorozirconate fibre, and so can be used only in laboratory conditions.

Amplification of 632.8 nm signals has also been achieved [48], in Pr^{3+}- optical fibre, from the $^3P_0 \rightarrow {}^3F_2$ transition. Illumination with a wavelength of 476.5 nm, from an argon-ion laser, was required to populate the ^3P manifold. Gains of up to 11 dB were achieved, despite the fact that the system was not fully optimised.

In the temperature-sensing field, the fluorescence lifetime variation of certain transitions in various Pr^{3+}-doped fluorozirconate (with additional phosphorous) bulk glass samples of different concentrations were investigated by Nguyen *et al.* [49]. This investigation suggests that at one concentration the fluorescence lifetime would be independent of temperature, thus Pr^{3+}-doped fluorozirconate fibre could become a dedicated strain sensor, as discussed in the next chapter.

3.5 Conclusion

Rare-earth-doped materials have been essential in optical applications that include fibre lasers, optical amplifiers and sensors. This is due to the 4f electron orbital that is shielded from outside influences, resulting in absorption and fluorescence peaks that are both narrow and relatively weak, when compared to transition metals that have broad and strong absorption and fluorescence peaks.

The Pr^{3+} ion has three metastable energy levels. These are the ^3P manifold, $^1D_2$ and $^1G_4$, and these allow a wide range of laser wavelengths and efficient amplification at the 1.3 μm telecommunications wavelength, when compared to Nd^{3+}-doped optical fibre. There has also been speculation with Pr^{3+}-doped fluorozirconate glass samples that a temperature independent strain sensor can be created; this has the potential to simplify strain measurement systems relying on fluorescence lifetime techniques.

4 Theory of fluorescence lifetime measurements

4.1 Chapter overview

In the previous chapter, examples were provided of where certain fluorescence transitions could occur in some materials and not in others; this is the result of competing effects within the material when illuminated with light.

There are two types of transitions that can occur in an optically active ion, radiative, otherwise known as fluorescence, and non-radiative, which can be in the form of phonon emission and cross-relaxation mechanisms. This chapter will discuss the properties of fluorescence and phonons, as well as the effect that the host material has on these transitions. Fluorescence measurements from various Pr^{3+}-doped materials will also be reviewed.

4.2 Fluorescence

Fluorescence occurs when matter (eg. phosphor, rare-earth ion) with excess energy, releases a photon in order to return to a lower energy state. Usually the emitted photon is of lower energy than the excitation "pump" photon energy. As shown as figure 4.1 (a), a photon with energy (hν), is incident on an atom thereby exciting it. The ion naturally decays to its ground state energy level and can do this by emitting a fluorescence photon (figure 4(b)). Fluorescence photons are isotropic in nature, have no preferred polarisation orientation and have a different phase to that of the incident (pump) photon.

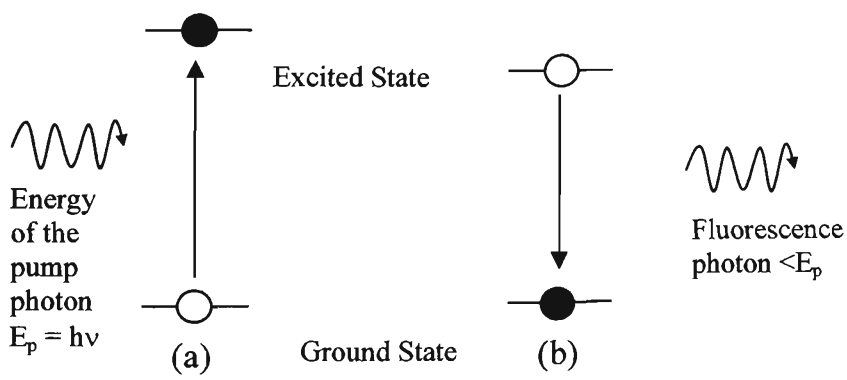

Figure 4.1 *(a) Absorption of a photon E=hν, and (b) the fluorescence photon which has less energy than the pump photon. The open circle represents the state of the ion before interaction, and the solid circle represents the ion's state after interaction.*

Fluorescence can be utilised in many different ways; the intensity of fluorescence can be used to measure the radiative efficiency of particular energy levels, the fluorescence lifetime is inherently temperature dependent. This latter property has been developed commercially by Luxtron Corporation [50].

4.3 Measuring the fluorescence lifetime

When a large number of ions are promoted into excited states, the fluorescence that is emitted is not released at exactly the same time; rather, the intensity of fluorescence as a function of time can be described as:

$$I(t) = I_0 \exp -(t/\tau), \tag{4.1}$$

where I_0 is the initial intensity, time is denoted by t, and τ is the fluorescence lifetime. Fluorescence lifetime is defined as the time taken for fluorescence intensity to decrease to 1/e of its original intensity, as shown in figure 4.2. The measured fluorescence lifetime, in this example is of the order of 130 μs. If several fluorescence transitions emanate from the same energy level, but terminate at different energy levels, then all the measured fluorescence lifetimes would be identical. There are several methods to measure the lifetime of fluorescence decay, some of which have been outlined by Grattan and Zhang [1].

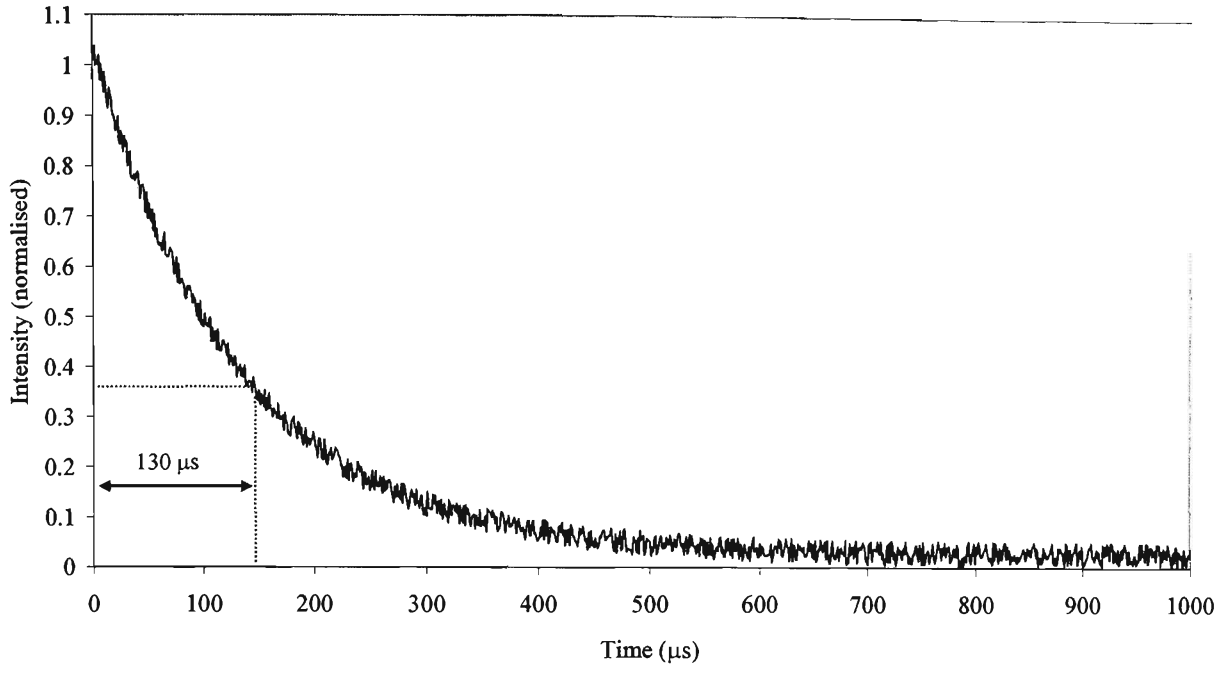

Figure 4.2 *An illustration showing fluorescence intensity decay over time, its associated lifetime is calculated by measuring the time taken for the fluorescence intensity to drop by 1/e of the initial fluorescence intensity, in this case 130 µs.*

4.4 Non-radiative processes

Fluorescence transitions have competing effects that reduce their efficiency; these are collectively known as non-radiative processes. This section will look at the effects of phonon decay, which are vibrational modes in the glass lattice that dissipate energy, and cross-relaxation mechanisms that reduce fluorescence efficiency and alter the measured fluorescence lifetime.

4.4.1 Phonon emission

It has been found by other researchers found that excited energy levels that were close to lower energy levels, were less likely to produce fluorescence; this was interpreted that energy was emitted non-radiatively, by what is known as phonon decay, to the host material [51], as illustrated in figure 4.3.

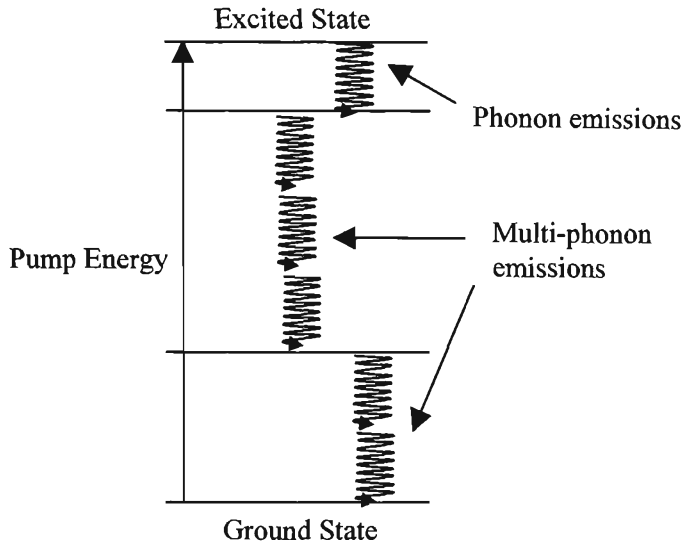

Figure 4.3 *Phonon emission between the energy levels of a fictitious rare-earth ion. There would be no fluorescence in this situation.*

Energy gaps that are about the energy of one or two phonons decay readily to lower energy levels, as shown in figure 4.3. Phonons can also bridge energy gaps that require more than two phonons. This is known as a multi-phonon relaxation and was first described by Kiel [37] in crystalline solids and further expanded by Riseberg and Moos [51]. Multi-phonon relaxation, although weaker, being a higher-order electromagnetic process, can become a serious issue, as the electron-phonon interaction is much greater, by eleven orders of magnitude, than electron-photon processes [37]. However, as the number of phonons required to bridge the gap increases, the non-radiative rate, W_{nr}, decreases dramatically, as shown in equation 4.3.

$$W_{nr} = C(n(T)+1)^{p} e^{(-\alpha \Delta E)}. \tag{4.3}$$

In this expression C and α are host-dependent parameters [52] (see table 4.1), ΔE is the energy gap between levels, p represents the average number of phonons required to bridge the gap, and $n(T)$ is the Bose-Einstein occupation number for the effective phonon mode [52], given by

$$n(T) = (\exp(\hbar\omega/kT) - 1)^{-1}, \tag{4.4}$$

where, ω is the phonon angular frequency. The non-radiative rate increases with increasing temperature because of the temperature dependent term in $n(T)$. However,

lowering the temperature will not decrease the non-radiative rate because the exponent p is small with levels that have a small energy gap. The parameters C and α are empirical values that are host dependent and are insensitive to the rare earth ion and the energy levels involved. They are obtained by fitting Eq. (4.2) to the non-radiative rates observed for as many energy gaps as possible using different levels and ions in the same host. Reisfeld and Jørgensen [53] have assembled these parameters from a large number of authors, and the values are shown in table 4.1, along with crystalline LaF_3 (for comparison).

Table 4.1 *Parameter values to use in conjunction with equation 4.2 and 4.3 [53]. C and α are empirical values independent of host material and $\hbar\omega$ is the energy of a single phonon in a particular material. Crystalline materials (eg. LaF_3) have lower phonon energies than amorphous materials (eg. silicate).*

Host glass	C (s^{-1})	α (10^{-3}) (cm)	$\hbar\omega$ (cm^{-1})
Borate	2.9×10^{12}	3.8	1400
Phosphate	5.4×10^{12}	4.7	1200
Silicate	1.4×10^{12}	4.7	1100
Germanate	3.4×10^{12}	4.9	900
Tellurite	6.3×10^{12}	4.7	700
Fluorozirconate	1.59×10^{12}	5.19	500
Sulfide	10^{6}	2.9	350
LaF_3	6.6×10^{8}	5.6	350

Oxide-based glasses have a larger non-radiative rate due to their strong covalent bonds that result in higher phonon frequencies; therefore, they are opaque at longer wavelengths. Crystalline hosts that have weaker ionic bonds lead to lower non-radiative rates due to lower $n(T)$ values and this indicates that these materials have greater transparency at longer wavelengths compared with oxide-based glass.

4.4.2 Cross-relaxation processes

Cross-relaxation is another means of energy dissipation between two ions. An ion in an excited state (donor) transfers part of its energy to a neighbouring ion (acceptor)

[37]. After transferral of energy, the donor and/or acceptor ions can release residual energy through phonon emission because the final energy levels are closely separated,

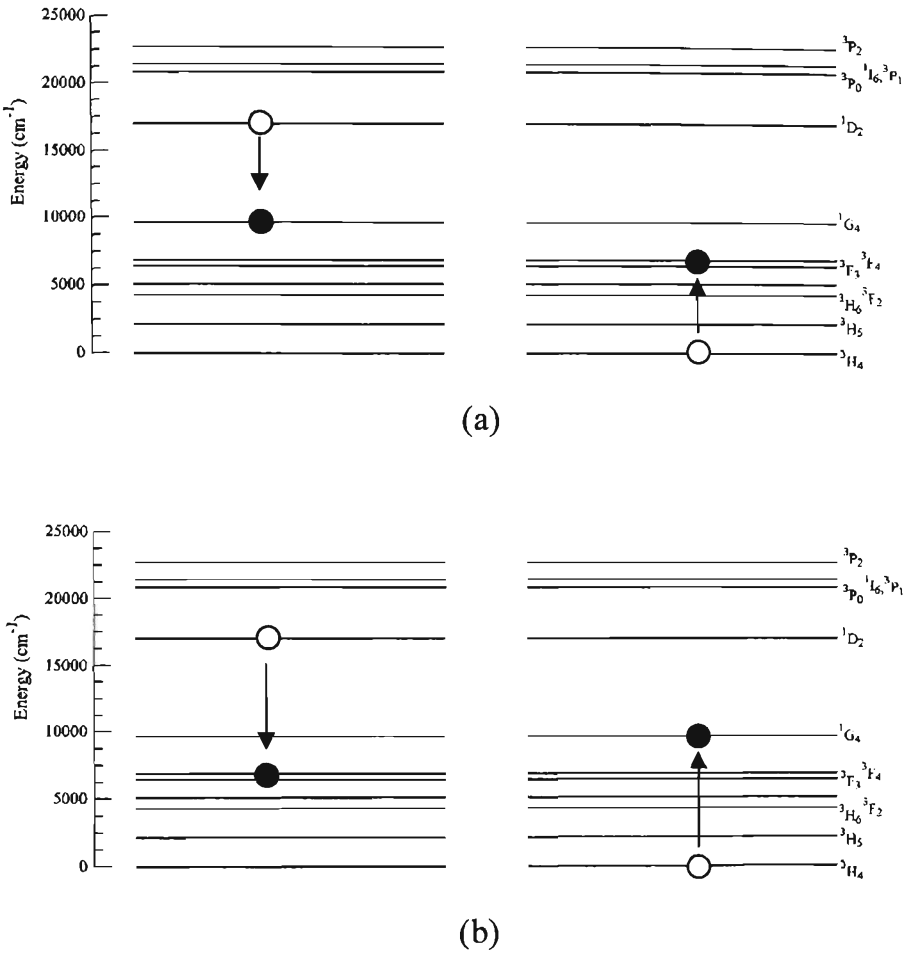

Figure 4.4 *Two ion processes that can occur in Pr^{3+}-doped materials; these processes lead to an decrease in fluorescence lifetime. The open circles are the position of the ions before the transition occurs, and the closed circles are the positions of the ions after the cross-relaxation has taken place.*

as illustrated in figures 4.4 (a). In these figures, the open circle represents the initial state of the ion and the closed circle represents the final state of the ion.

The energy levels in Pr^{3+} ions in a silica host are separated such that the lower energy states relax to the ground state by phonon emission. The illustrations in figure 4.4 (a) and (b) illustrate two two-ion cross-relaxation processes.

Rare-earth dopants have the tendency to disperse inhomogenously, because rare-earth ions are unable to position themselves effectively within the silica matrix. This results in regions where large numbers of rare-earth ions are located, known as clusters. A

consequence of clustering amongst rare-earth ions in silica glass is that cross-relaxation occurs more readily. One method to alleviate this problem is to introduce aluminium oxide during the production of rare-earth-doped optical fibre [37]. Rare-earth ions are soluble in aluminium oxide, which in turn is soluble in the silica matrix. The distribution of the rare-earth ion becomes more homogenic in the core of the optical fibre and decreases the cross-relaxation effects, as the aluminium oxide creates areas within the glass structure where the rare-earth ion can be positioned. The inclusion of aluminium oxide also allows the rare-earth ions to have greater concentration in the centre of the core thereby improving the performance of fibre lasers and sensors.

4.5 Temperature effects on the fluorescence lifetime

Fluorescence lifetime temperature measurements often take advantage of the energy gap between two thermalised levels [26]. An energy level diagram for such a pair of levels, in a rare-earth ion, is shown in figure 4.5.

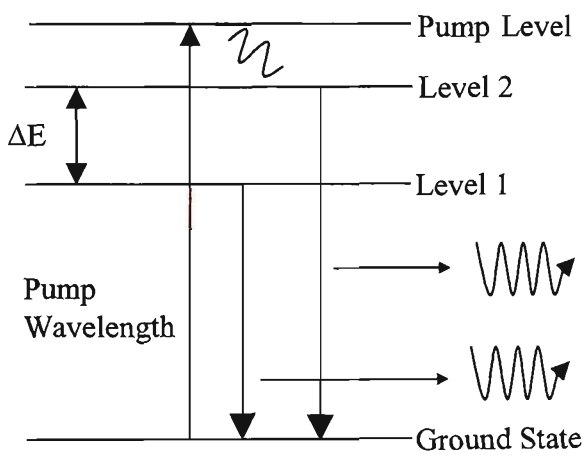

Figure 4.5 *An energy level diagram of a rare-earth ion demonstrating the fluorescence radiating from a pair of thermalised energy levels, via a phonon decay into radiating level.*

Figure 4.5 represents the pumping scheme used to populate the thermalised Stark levels within the $^1D_2$ energy level of the Pr^{3+} ion. In this case the ratio of the population distribution amongst these levels, when pumped, is described by the population level 2 (n_2) to that of level 1 (n_1), is given by the ratio of the degeneracies (g_1 and g_2) and the Boltzmann factor as given in equation 4.5

$$\frac{n_2}{n_1} = \frac{g_2}{g_1}\exp\left(-\frac{\Delta E}{kT}\right), \tag{4.5}$$

where ΔE is the energy gap between the thermalised levels, and T is the absolute temperature.

The exponential term is effectively a weighting factor for the population of the upper energy level to that of the lower energy level. When thermalised, these levels (1 and 2) have the same fluorescence lifetime, given by equation 4.6

$$\tau = \frac{1+\frac{g_2}{g_1}\exp\left(-\frac{\Delta E}{kT}\right)}{w_{10} + w_{20}\frac{g_2}{g_1}\exp\left(-\frac{\Delta E}{kT}\right)}, \tag{4.6}$$

where w_{10} and w_{20} are the temperature-independent decay rates of the two levels. The temperature dependence of the lifetime is due to the population distribution amongst the thermalised energy levels and is heavily dependent on the phonon behaviour of the host material.

Figure 4.6 shows the lifetime response of Cr^{3+}-doped fibre with temperature [1]. The lifetime measurements are shown by asterisks, the dashed line illustrates the lifetime trend, and the solid line shows the fit to these data from equation 4.6 using a least squares fitting.

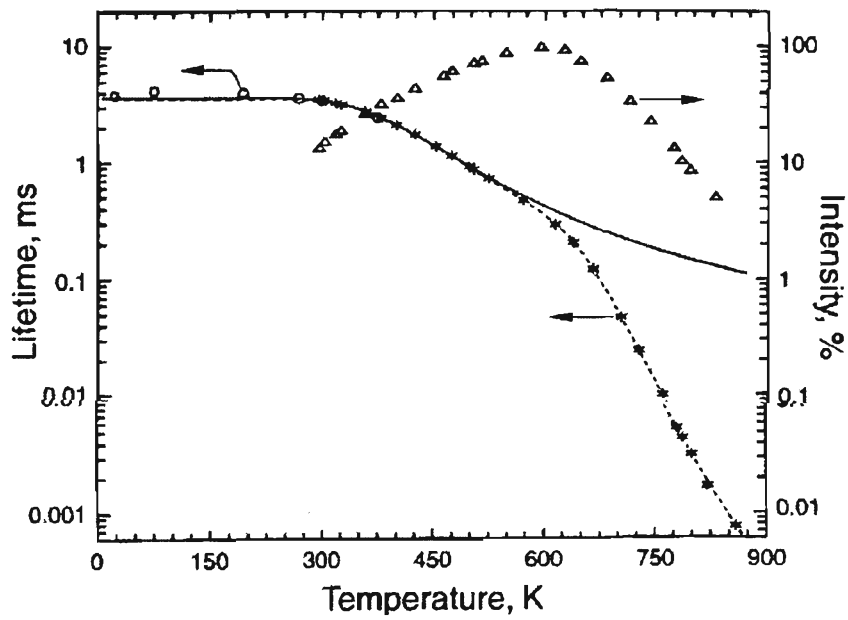

Figure 4.6 *Fluorescence lifetime and intensity measurements of Cr^{3+}-fluorescence in ruby crystal [1]. The solid line is a fit using equation 4.6.*

Also shown in the axis on the right hand side in figure 4.6 is the intensity of fluorescence as an indication of the population change for the detected energy level. As seen for the fitted data for lifetime, equation 4.6 follows the lifetime-temperature trend very well at temperatures below 550 K. However, above this temperature the equation deviates from the data trend, because there is no inclusion of phonon decay in equation 4.6.

An equation that allows phonon interaction to be included was produced by Zhang *et al.* [54] to describe the lifetime variance of alexandrite and Yb^{3+}-based temperature sensors up to a temperature of 700 °C. This is similar to equation 4.6 but with an extra term to describe the phonon interaction of the host material as described in equation 4.7;

$$\tau = \frac{1+\frac{g_2}{g_1}\exp\left(-\frac{\Delta E}{kT}\right)}{w_{10}+w_{20}\frac{g_2}{g_1}\exp\left(-\frac{\Delta E}{kT}\right)+w_q\exp\left(-\frac{\Delta E_q+\Delta E}{kT}\right)}. \qquad (4.7)$$

From this equation, the effect of phonon decay that is evident at high temperature can be fitted with greater accuracy than with equation 4.6. The inclusion of w_q, and ΔE_q terms allow the rates of thermally quenched processes and its effective energy gap to

be included in the fluorescence lifetime equation. Higher values of ΔE_q suggest that the process is dominated by phonon interactions, as well as large values of w_q, which indicate a fast energy transfer.

The effects that parameters w_{10} and w_{20} have on fluorescence lifetime have been collated by Collins *et al.* [55] for various rare-earth and transition metal -doped optical fibre temperature sensors. Nguyen *et al.* [49] measured the fluorescence lifetime-temperature dependence originating from the $^3P_0$ level in Pr-doped ZBLANP bulk samples. Fitting the parameters w_{10} and w_{20} as a function of concentration, ρ, found that w_{10} was concentration independent, whereas w_{20} was found to be concentration dependent and followed a quadratic fit. This allowed, equation 4.7 to be re-written:

$$\tau = \frac{1+\frac{g_2}{g_1}\exp\left(-\frac{\Delta E}{kT}\right)}{w_{10}+\left(\alpha+\beta\rho+\gamma\rho^2\right)\frac{g_2}{g_1}\exp\left(-\frac{\Delta E}{kT}\right)}, \tag{4.8}$$

where α, β and γ are concentration dependent fluorescence lifetime rates for Pr^{3+}-doped fluorozirconate bulk glass samples. This model was used successfully to describe the effect of rare-earth concentration on fluorescence lifetime–based temperature sensing in Pr-doped ZBLANP bulk samples. The measurements indicate that fluorozirconate bulk glass with a Pr^{3+}-ion concentration of 6900 ± 200 ppm should result in fluorescence lifetimes that have close to zero temperature dependence; this result was confirmed by Vella *et al.* [56]. Fluorescence lifetime measurements of Pr^{3+}-doped fluorozirconate in fibre have yet to be conducted in the same conditions.

4.6 Strain effects on fluorescence lifetime

Axial strain through the fibre also affects the fluorescence lifetime of an excited energy level in a rare-earth ion (section 2.3.2.4). An investigation of Nd^{3+}-doped silica fibre [57] demonstrated that fluorescence lifetime has strain dependence, but did not give an explanation on the origin of this dependence. Tröster *et al.* [58] found that

when Cl_3 crystals doped with Nd^{3+} or Pr^{3+} ions were subject to very high pressure a slight shift in the observed energy level occurred. The fluorescence lifetime-strain sensitivity has also been attributed to a volumetric distortion of the energy transfer rates between the dopant ions, in which increasing strain along a fibre results in a slight reduction of concentration [59]. This mechanism, which should be detectable at strains that can be withstood by optical fibres unlike the effect that Tröster described, is discussed later.

Arguments have also been presented that discount shifts in ΔE as the cause of this strain dependence. Farrell *et al.* [59] obtained an expression for the strain-temperature cross-sensitivity, β (ie strain sensitivity divided by the temperature sensitivity) for both the fluorescence intensity ratio and fluorescence lifetime techniques, namely

$$\left(\frac{\partial R}{\partial \varepsilon}\right)\Big/\left(\frac{\partial R}{\partial T}\right)=\left(\frac{\partial \tau}{\partial \varepsilon}\right)\Big/\left(\frac{\partial \tau}{\partial T}\right)=-\frac{T}{\Delta E(\varepsilon)}\frac{\partial \Delta E(\varepsilon)}{\partial \varepsilon}. \tag{4.9}$$

This suggests that the strain-temperature cross-sensitivity for both fluorescence intensity ratio and fluorescence lifetime should be identical, as the result is the same for both sensor-types. The fact that equation (4.9) does not agree with experimental results, as strain sensitivities for fluorescence intensity ratio measurements have been found to be an order of magnitude less than those for fluorescence lifetime measurements [26], eliminates shifts in ΔE as the cause of strain dependence.

Farrell *et al.* analysed the strain-induced reduction in concentration as follows. Strain applied to optical fibre is given by the unstrained fibre's length (L), or unstrained fibre volume (V), and the change in the fibre's length (ΔL) or volume (ΔV),

$$\varepsilon=\frac{\Delta L}{L}=\frac{\Delta V}{V}. \tag{4.10}$$

The volume distortion resulting from strain is considered to have negligible effect on the fibre's cross-sectional area. The concentration of rare-earth ions (ρ) in the fibre is a function of the number of rare-earth ions (n) per unit volume (V), and is described by

$$\rho=\frac{n}{V}. \tag{4.11}$$

The change that the rare-earth ion concentration experiences due to a change in volume, from an applied strain, is given by

$$\frac{\partial \rho}{\partial V} = -\frac{n}{V^2} = -\frac{\rho}{V}. \tag{4.12}$$

The negative sign indicates that increases in volume results in a lower rare-earth ion concentration. Expansion of equation (4.9) and substitution of equation (4.11) gives

$$\varepsilon = \frac{\Delta V}{\Delta \rho} \cdot \frac{\Delta \rho}{V} = -\frac{V}{\rho} \cdot \frac{\Delta \rho}{V} = -\frac{\Delta \rho}{\rho} = \frac{\rho_0 - \rho(\varepsilon)}{\rho_0}, \tag{4.13}$$

where rare-earth ion concentration under zero strain is given by (ρ_0), and $\rho(\varepsilon)$ is the concentration of rare-earth ions when that fibre is under strain. Equation (4.13) can be rearranged to give

$$\rho(\varepsilon) = \rho_0(1-\varepsilon). \tag{4.14}$$

Cross-relaxation between two ions (dipole interaction) is proportional to the inter-ion distance (R) by a $1/R^6$ relationship [60]. Hence, when fibre is under strain, the distance between these dipole as a function of strain is

$$R(\varepsilon) = R_0 + \Delta R = R_0\left(1 + \frac{\Delta R}{R}\right) \tag{4.15}$$

and $\Delta R/R$ is the definition of strain (from equation (4.10)). The $1/R^6$ term can be expressed as

$$\frac{1}{R^6} = \frac{1}{R_0(1+\varepsilon)^6} \approx \frac{1}{R_0^6}(1-6\varepsilon). \tag{4.16}$$

to first order (ie, neglecting terms in ε^2 and higher). Analogously, a three ion dipole interaction is described by the following

$$\frac{1}{R^{12}} = \frac{1}{R_0(1+\varepsilon)^{12}} \approx \frac{1}{R_0^{12}}(1-12\varepsilon). \tag{4.17}$$

In equation (4.8), the coefficients β and γ are used to describe a two and three ion cross-relaxation process, respectively, for the $^3P_0$ level in Pr-doped ZBLANP host.

w_{20}, which in equation 4.8 was replaced by a quadratic dependence upon ρ, becomes (by substitution of equations (4.14, 4.16 and 4.17))

$$w_{20} \propto \left(\alpha + \beta_0\rho_0(1-\varepsilon)(1-6\varepsilon) + \gamma_0\rho_0^2(1-\varepsilon)(1-12\varepsilon)\right), \tag{4.18}$$

which can be reduced to

$$w_{20} \propto \left(\alpha + \beta_0\rho_0 - \varepsilon(7\beta_0\rho_0 + 12\gamma_0\rho_0^2)\right) = w_{20}^{'} + k_{20}\varepsilon\,, \tag{4.19}$$

assuming the applied strain is small. This leads to a linear dependence in strain on the cross-relaxation transition rate for rare-earth ion dipole interaction from the $^3P_0$ and $^3P_1$ energy levels in Pr-doped ZBLANP host material, when only first order effects are considered. Hence it was predicted that the effect of strain on fluorescence lifetime on the $^3P_0$ level in Pr-doped ZBLANP fibre is

$$\tau = \frac{1+\frac{g_2}{g_1}\exp\left(-\frac{\Delta E}{kT}\right)}{\left(w_{10}\right)+\left(w_{20}^{'}+k_{20}\varepsilon\right)\frac{g_2}{g_1}\exp\left(-\frac{\Delta E}{kT}\right)}. \tag{4.20}$$

However there are no data to confirm this prediction for the $^3P_0$ energy level.

The arguments leading to a simple linear dependence of the transition rate upon strain, ie, equation (4.19) arose from details of 2- and 3- ion processes. This suggests that for a situation in which there is no knowledge of decay processes, a similar dependence for both w_{10} and w_{20} should be investigated. Therefore the following equation will be used to fit results for the $^1D_2$ energy level in Pr^{3+} -doped silica optical fibre

$$\tau = \frac{1+\frac{g_2}{g_1}\exp\left(-\frac{\Delta E}{kT}\right)}{\left(w_{10}^{'}+k_{10}\varepsilon\right)+\left(w_{20}^{'}+k_{20}\varepsilon\right)\frac{g_2}{g_1}\exp\left(-\frac{\Delta E}{kT}\right)}. \tag{4.21}$$

Through the use of equation (4.21), it may be possible to determine if there is any fluorescence lifetime-strain dependence on the fluorescence lifetime rates (w_{10} and w_{20}) for the $^1D_2$ energy level in Pr^{3+} -doped silica optical fibre.

4.7 Strain-temperature cross-sensitivity

The previous sections (4.6 and 4.7) have shown that fluorescence lifetime is sensitive to both temperature and strain. According to Collins *et al.*, "the temperature response of the fluorescence lifetime technique can be approximated quite well by a linear response over a certain range, so that they can be characterised by their average sensitivities, $\partial\alpha/\partial T$ and $\partial\alpha/\partial\varepsilon$, where α is the fractional change in the quantity being measured in the region of interest [26]." The strain-temperature cross-sensitivity (β) can be defined as

$$\beta = \frac{\partial\alpha}{\partial\varepsilon} \Big/ \frac{\partial\alpha}{\partial T}. \tag{4.22}$$

When equation 4.11 is equal to zero, this implies the sensor over a specific range was strain independent. Temperature and strain fluorescence lifetime measurements of Nd^{3+}-doped silica optical fibre of various concentrations were obtained. Figure 4.7 shows how strain-temperature cross-sensitivity was affected by concentration. These were fitted using an equation similar to equation (4.8) ($w_{10} = a + b\rho$ *and* $w_{20} = c + d\rho^2$), believed to be appropriate for the energy levels in Nd^{3+} [61].

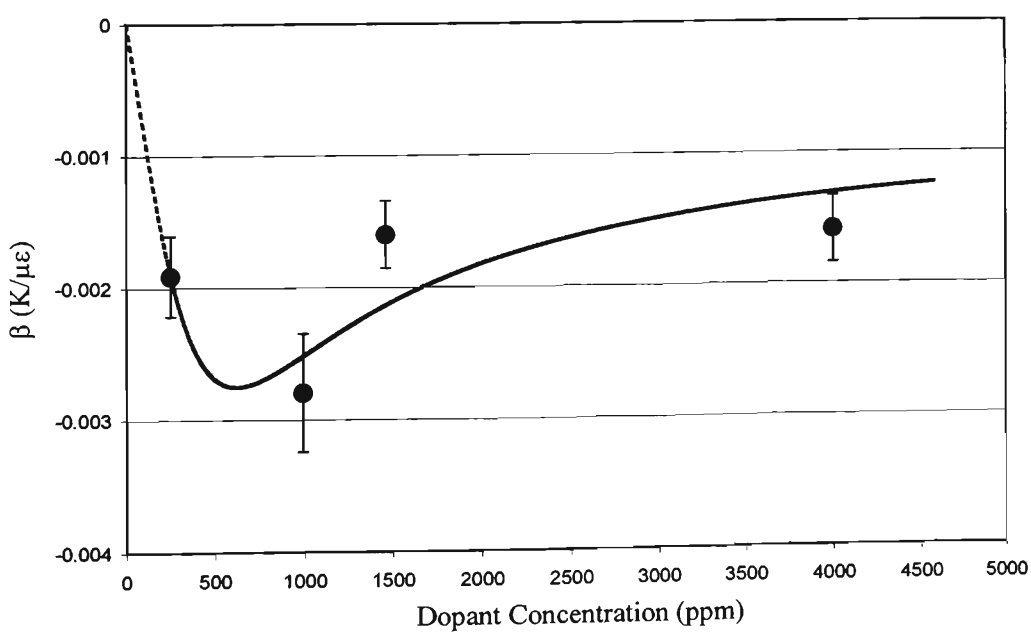

Figure 4.7 *A model describing the strain-temperature cross-sensitivity of Nd^{3+}-doped silica optical fibre [after, [61]].*

The model predicts that the strain-temperature cross-sensitivity has a negative value for Nd^{3+}-doped silica fibre; the dependence on the Nd^{3+}-ion concentration data is in accordance with the trend of the model. This is very encouraging but, as the fibre compositions may be dissimilar (as they came from different batches), this finding must be treated with caution. Strain-temperature cross-sensitivity values of Nd^{3+}, Er^{3+}, Yb^{3+} and Pr^{3+}(from this thesis)-doped silica optical fibres are shown in Section 7.3. It should also be noted that this model did not predict the correct sign of the very small strain-temperature cross-sensitivity value of Nd^{3+}-doped silica optical fibre fluorescence intensity ratio data [61].

4.8 Fluorescence lifetime measurements from Pr^{3+}-doped materials

The fluorescence properties of Pr^{3+}-doped materials have been studied in many host materials. Table 4.2 shows some of the materials studied and the fluorescence lifetimes for the associated transitions are shown.

Table 4.2 *A comparison of praseodymium-doped materials showing transitions, materials and temperature ranges*

Host	Transition	Lifetime (μs)	Temperature range (K)	Ref.
Br_3	$^3P_0 \rightarrow {}^3H_4$	1.0 - 0.95	0 - 300	[62]
Cadmium-Fluorochloride	$^1G_4 \rightarrow {}^3H_5$	332	NA	[45]
Cl_3	$^3P_0 \rightarrow {}^3H_4$	11.5 - 0.5	0 - 300	[62]
Cs:Ga:S:Cl	$^3P_0 \rightarrow {}^3H_4$	61	NA	[46]
	$^1D_2 \rightarrow {}^3H_4$	700	NA	
	$^1G_4 \rightarrow {}^3H_4$	2460	NA	
$LiYF_4$ (0.1% Pr)	$^1D_2 \rightarrow {}^3H_4$	870 - 400	4 - 300	[63]
$LiYF_4$ (1% Pr)	$^3P_0 \rightarrow {}^3H_4$	50 - 30	4 - 500	[63]
	$^1D_2 \rightarrow {}^3H_4$	630 - 300	4 - 600	
Pr(0.01) La(0.99) Br_3	$^3P_1 \rightarrow {}^3H_4$	7.2 - 2.5	4 - 300	[64]
	$^3P_0 \rightarrow {}^3H_4$	122 - 10.5	4 - 300	
Pr(0.001)La(0.99)Cl_3	$^3P_1 \rightarrow {}^3H_4$	2.5 - 0.9	4 - 300	[64]
	$^3P_0 \rightarrow {}^3H_4$	14.7 – 12	4 - 300	
Silica	$^1D_2 \rightarrow {}^3H_4$	120	NA	[40]
Silica:Al_2O_3	$^1D_2 \rightarrow {}^3F_{3,4}$	205	NA	[65]
Tellurite	$^3P_1 \rightarrow {}^3H_5$	10.4	NA	[47]
	$^3P_0 \rightarrow {}^3H_5$	9.6	NA	
	$^1D_2 \rightarrow {}^3H_5$	139.6	NA	
ZBLA	$^3P_1 \rightarrow {}^3H_5$	13	300	[66]
	$^1P_0 \rightarrow {}^3H_5$	15	300	
	$^1D_2 \rightarrow {}^3H_4$	55	300	
ZBLAN	$^3P_0 \rightarrow {}^3F_{3,4}$	15	NA	[41]
	$^1G_4 \rightarrow {}^3H_5$	155 – 90	4 - 340	[42]

Table 4.2 shows that some transitions are allowed for particular host materials, but not for others; this has already been discussed (section 4.4). The fluorescence lifetime is also host dependent. For example, Pr^{3+}-doped Cs:Ga:S:Cl has a $^1D_2 \rightarrow {}^3H_4$ transition lifetime of 700 μs, whereas the same transition for Pr^{3+}-doped ZBLA has 55 μs and for Pr^{3+}-doped silica it is 120 μs.

Figure 4.7 shows the energy level diagram for Pr^{3+}-doped fluorozirconate glass; these energy levels would not change significantly to that of a silica host. The energy gap differences between $^3P_0$ and $^1D_2$ ($\approx$ 3800 cm^{-1}) indicates that the majority of transitions would be non-radiative as three phonons are required to bridge this gap. An increase in temperature will result in an increase in the phonon decay rate (equation 4.3), further reducing any fluorescence emanating from this level. Similarly, any transitions from the $^1G_4$ energy level would result in little fluorescence as the energy gap to the next level down, $^3F_4$, has a separation of $\approx$ 3100 cm^{-1}. The majority of fluorescence from the Pr^{3+}-doped silica host would occur from the $^1D_2$ level as the

energy gap to the $^1G_4$ energy level is ≈ 7200 cm^{-1} resulting in strong fluorescence that would weaken as temperature increases. Indeed Percival *et al.* [40] has measured that the majority of fluorescence peaks emanating from Pr^{3+}-doped silica results from the $^1D_2$ energy level (section 3.4). The measurements in this thesis involve the fluorescence that results from transitions originating from the $^1D_2$ energy level and all transitions originating from this energy level will have the same fluorescence lifetime.

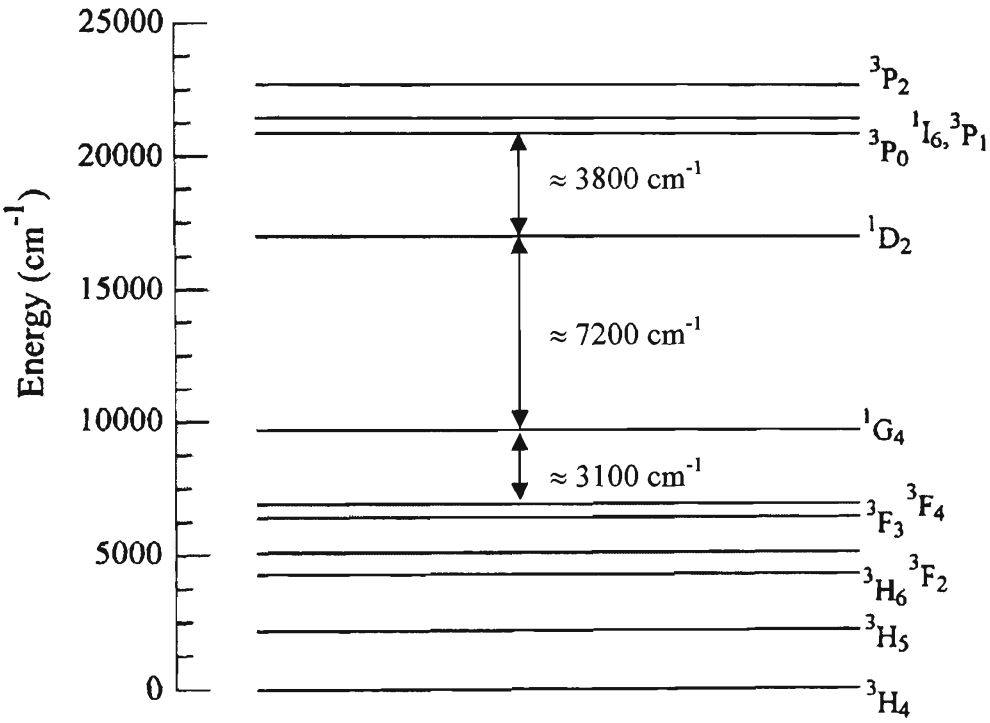

Figure 4.8 *A typical energy level diagram for Pr^{3+}-doped glass [after [67]].*

4.9 Conclusion

Ions in excited states can return to their ground state by radiative, non-radiative, or a combination of the two processes. Fluorescence is the release of excess energy in the form of a photon that has lower energy than the excitation energy. The released photon is isotropic in nature, has no preferred polarisation orientation and can be of a different phase from the excitation photon.

Non-radiative processes include phonon emissions that are host dependent, crystalline hosts have lower phonon energy than that of an amorphous host; this is a direct result of the structure of the material. Cross-relaxation processes transfer energy from a

donor ion to an acceptor ion occur more readily where rare-earth dopants are clustered and are therefore in closer proximity.

Temperature affects fluorescence lifetime mainly from an increase in phonon emission at elevated temperatures, as described in equation 4.7. The concentration of rare-earth dopants in the glass can also affect the fluorescence lifetime–temperature sensitivity as described by Nguyen *et al.* [49].

Strain has also been found to affect the fluorescence lifetime; theories are still developing to determine how this is possible. A model by Farrell *et al.* [59] suggests that fluorescence lifetime is most likely not caused by shifts in the energy level, but by changes in the fluorescence rates (w_{10} and w_{20}) associated with reduced cross-relaxation due to reduced concentration. Fits to the Nd^{3+} fluorescence lifetime data, provide some support for this model. It should, however, be noted that the model did not account for the Nd^{3+} fluorescence intensity ratio data.

The transitions from the three energy level manifolds in Pr^{3+}-doped silica were described in terms of both energy gap and phonon energy. The $^1D_2$ energy level should show a high fluorescence intensity when compared to the $^3P_0$ and $^1G_4$ energy levels, which fits into the work described by Percival *et al.* [40].

5 Experimental detail

5.1 Introduction

This chapter details optical arrangements, and the software and hardware parameters, that were used to conduct measurements of the fluorescence lifetime of Pr^{3+}-doped optical fibre under a variety of external temperatures and applied strain.

Figure 5.1 shows the optical layout used for temperature and strain sensing. An argon-ion laser (Spectra-Physics, Stabilite 2017-05S) was operated at 488 nm and had a beam diameter of 5.6 mm and an output power of 1.5 W. Since direct modulation of a gas laser is detrimental to its operational lifetime, an acousto-optic modulator (AOM) was used. A 500 Hz square wave signal from a function generator was used for both the AOM and as the trigger source for an oscilloscope.

The modulated beam entered the single mode dummy fibre through a microscope objective (×20), whose other end was fusion spliced to the Pr^{3+}-doped fibre. During strain tests, additional telecommunication grade fibre was spliced onto the other end of the Pr^{3+}-doped fibre. Weights were applied to this fibre to provide strain on the doped fibre section.

Only fluorescence counter-propagating to the pump direction was analysed. This fluorescence travelled back through the microscope objective (where it was collimated) and entered a multi-mode fibre that is orthogonal to the pump laser beam path via a cubic beam splitter and another microscope objective (×10). A long pass and a band pass filter were used to block any stray pump light, and to admit only a specific fluorescence peak to the detector.

Depending upon the fluorescence wavelength the fluorescence was detected by either a photomultiplier tube (PMT) or an InGaAs photodiode (PD), and the decay curve was captured on a digital oscilloscope (Tektronix TDS 320).

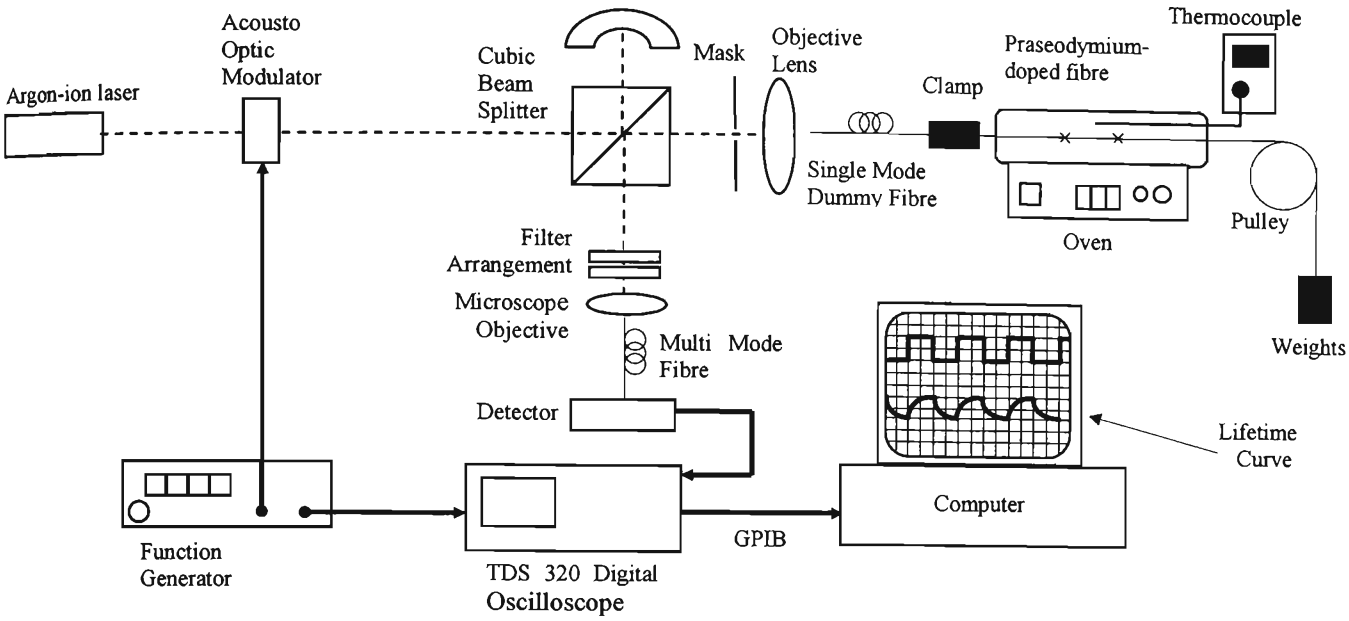

Figure 5.1 *Schematic diagram of the optical arrangement. Temperature tests were conducted with zero strain on the fibre. Strain tests were conducted at room temperature, albeit with no heater.*

5.2 Apparatus detail

5.2.1 Argon-ion laser

The Argon-ion laser (Spectra Physics 2017-05S) has variable power control from 75 mW up to 2 W at a wavelength of 488 nm; this wavelength was the best suited from both previous work [39,40] and from preliminary measurements.

There are two ways to operate this particular argon-ion laser, by either current or power control. Current control stabilises the specified current that drives the laser irrespective of the output power. Since power fluctuations can occur during measurements, this mode was used for preliminary optical alignment only.

Power control detects the output power of the laser via a photodiode that is connected to a feedback circuit that adjusts the current to suit the nominated power level. Care must be taken in this mode, so that the current does not exceed the maximum rating, most experiments had the laser with an output power of 1.5 W.

5.2.2 Acousto-optic modulator

An acousto-optic modulator (AOM) works on the basis that some crystals exhibit photo-elastic processes to couple acoustic waves into the crystal that one wishes to modulate. These acoustic waves operate in a similar fashion to Bragg scattering, allowing the light to be modulated at the frequency of the acoustic wave.

In this investigation, an IntraAction Corp (AOM-40) AOM was utilised with an input frequency of 500 Hz with square wave modulation. The AOM was angled to allow good definition between the 0^{th} and 1^{st} order diffraction beams. A consequence of an angled beam is that the 1^{st} order diffraction beam entering the optical fibre will have less aberration from the microscope objective resulting in a greater coupling efficiency into the optical fibre.

5.2.3 Beam splitter

The cubic beam splitter used was from Edmund Optics with side lengths of 50 mm. The surfaces were anti-reflection coated to allow maximum transmission; the beam splitter did not affect the polarisation of the pump or fluorescence wavelengths.

5.2.4 Pr^{3+}-doped fibre

Two fibre samples were used for the series of experiments reported in this thesis, with concentrations of 700 ppm and 1000 ppm, referred to here as Pr1 and PrAl respectively. Both samples were manufactured at the *Laboratorie de Physique de la Matière Condensée, Université de Nice,* France, by the modified chemical vapour deposition and solution doping technique (Section 3.2).

The Pr1 fibre had a core diameter of 2 μm and was slightly elliptical with a cladding diameter of 125 μm. A silicone-based sheath protected the fibre from direct handling and water moisture.

The PrAl fibre had core and cladding diameters of 6 and 125 μm, respectively. Aluminium oxide was added to the fibre core, to minimise clustering effects that occur when high concentrations of rare-earth ions are present in silica-based optical

fibres; the Pr^{3+} and Al_2O_3 -dopant concentrations were 1000/4000 ppm respectively [68].

5.2.5 Filters

Long pass and band pass filters were required to extract the relevant fluorescence wavelengths from the various peaks in the spectra. The long pass filters were used to block the pump wavelength from damaging the detectors and to allow wavelengths longer than 600 nm to pass. The filters, both provided by Melles Griot, had cut-off wavelengths of 590 nm (OG 570) and 550 nm (GG 495) and were placed in series to further attenuate the pump wavelength.

Band pass filters were used to isolate the various fluorescence wavelengths, enabling the interrogation of narrow portions of the fluorescence spectrum for lifetime studies. The two fluorescence peaks were centred at 630 nm and 870 nm. The filter for the 630 nm fluorescence peak had a FWHM of 40 nm centred at a wavelength of 632.8 nm with a peak transmission of 80%, this filter was provided by Ealing Electro-optics. The filter for the 870 nm fluorescence peak had a FWHM of 40 nm centred at a wavelength of 900 nm with a minimum transmission of 45%, was manufactured by CVI Laser Corporation. Both filters had a diameter of 12.5 mm.

5.2.6 Detection

The detectors used in these measurements were a photomultiplier tube (PMT) and a photodiode (PD), chosen to suit the fluorescence wavelength. The PD (PR-X-100k-IN-AC) manufactured by Femto measured the fluorescence peak centred around a wavelength of 870 nm. The PD consisted of InGaAs sensor material with a circular active detection diameter of 1 mm. The spectral detection for this PD ranged from 850 to 1700 nm and it had a 10 Hz to 100 kHz bandwidth. This photodiode also had a transimpedance gain of 1×10^7 V/A and a response time of 3.5 μs, which is less than 5% of the fluorescence lifetime emanating from the $^1D_2$ energy level of Pr^{3+}-doped silica fibre.

Measurement of fluorescence lifetime from the fluorescence peak centred on the 630 nm wavelength was conducted by a Hamamatsu (R928) PMT. This PMT had an extended range in the red/infrared region of the spectrum with a practical wavelength

range from 185 – 900 nm, peaking at a wavelength of 400 nm. Load resistance across the PMT's output changed its response time and overall sensitivity. The response time from a 2000 Ω load resistor was measured to equal 1615 ns, and this load resistance was used during fluorescence lifetime measurements.

5.2.7 Digital oscilloscope

The digital oscilloscope (Tektronix TDS 320) was used for observing and capturing the fluorescence intensity decay. With a bandwidth of 100 MHz, the traces recorded by this oscilloscope were transferred to a computer via a GPIB cable and stored for further analysis.

This oscilloscope also had an averaging feature, that was used when measuring weak fluorescence signals (especially from the 630 nm transition from Pr1 fibre); all signals were averaged 256 times, the highest averaging allowed. Data transferred to the computer had its lifetime measured using a least squares regression program (*Table Curve Fit v.5*).

5.2.8 Signal-to-noise ratio

Photo-detectors used in this thesis are able to detect light signals and amplify these signals, they also amplify noise that is inherent to their detection type. The two main sources of noise for photo-detectors are thermal and shot noise [69]. Thermal noise (also known as *Johnson* noise) originates within the photo-detector's load resistor. Electrons in the resistor are thermally agitated, creating a small alternating current even when no voltage is applied across the resistor. The average voltage across the resistor is zero, but the average thermal noise power within the resistor is described by

$$P_{TN} = 4kT\Delta f R_L , \tag{5.1}$$

where k = Boltzmann constant (J K^{-1}), T = absolute temperature (K), Δf = bandwidth (Hz) and R_L = load resistance (Ω). Thermal noise has uniform noise intensity across all frequencies, up to about 10 GHz [69].

In both PMT and PD photo-detectors shot noise is created from random electron generation and recombination of free electrons with holes (PD), or, electrons jumping escaping to another dynode (PMT). Shot noise can be described by

$$P_{SN} = 2e(i_S + i_D)\Delta f\,, \tag{5.2}$$

where e = electron charge (C), i_s = the average detector current (A), I_D = photo-detector dark current (A). Shot noise intensity is uniform over the system bandwidth. Shot noise is also dependent on the signal current, which is proportional to the amount of light incident on the photo-detector.

The signal current from a photo-detector can be described by

$$I_S = \rho P\,, \tag{5.3}$$

where ρ = photo-detectors responsivity (A/W) and P is the incident optical power (W). Consequently, the average electrical signal power is

$$P_{ES} = I_s R_L = \rho P R_L\,. \tag{5.4}$$

The signal to noise ratio (SNR) can be described from the ratio of equation (5.4) to equations (5.1) and (5.2),

$$SNR = \frac{P_{ES}}{P_{TN} + P_{SN}} = \frac{(\rho P)^2 R_L}{(4kT\Delta f R_L) + 2e(\rho P + I_D)\Delta F R_L}\,. \tag{5.5}$$

For the PD used during fluorescence lifetime measurements (section 5.2.6), using a typical value of $\rho = 0.75$ A/W, with a trans-impedance gain of 10^7 V/A, P is in units of nW (fibre length dependent), $R_L = 50\ \Omega$, $T = 296$ K, $I_D = 0.02$ nA, $\Delta f = 100$ kHz.

The PMT used during these measurements (section 5.2.6), had the following values: $\rho = 0.05$ A/W with internal gain estimated at 1000, P is in units of nW (fibre length dependent), $R_L = 2000\ \Omega$, $T = 296$ K, $I_D = 2$ nA, $\Delta f = 100$ MHz. The resultant electrical signal power, thermal noise power, shot noise power, SNR values for both photodiode and PMT are displayed in table 5.1.

Table 5.1 *Signal-to-noise ratio values for the temperature and strain measurements for the PMT and photodiode.*

Temperature Measurements							
Fibre (length)	**Photo-detector**	**Optical power (nW)**	**P_{ES} (μW)**	**P_{TN} (nW)**	**P_{SN} (fW)**	**SNR**	**SNR (dB)**
Pr1 (100 mm)	PMT	9	0.16	1.6	280	100	20
(100 mm)	Photodiode	14	15	16	45	960	30
PrAl (100 mm)	PMT	25	1.2	1.6	800	800	29
(100 mm)	Photodiode	24	46	16	80	2800	35
Strain Measurements							
Fibre (length)	**Photo-detector**	**Optical power (nW)**	**P_{ES} (μW)**	**P_{TN} (nW)**	**P_{SN} (fW)**	**SNR**	**SNR (dB)**
Pr1 (50 mm)*	PMT	7	0.1	1.6	220	60	18
(700 mm)	Photodiode	17	20	16	50	1400	32
PrAl (50 mm)*	PMT	20	0.8	1.6	640	490	27
(700 mm)	Photodiode	35	100	16	110	6000	38

* Strain measurements at elevated temperatures

A SNR value that is less than three indicates that the signal is swamped by noise from the detector and from external amplification sources. The discrepancies between power levels and their SNR value may be the result of improper alignment between the counter-propagating fluorescence with the microscope objectives, multimode fibre and the PD. Care was taken at all times during measurements to ensure that optical power levels were optimised.

5.3 Temperature measurement

Measurements requiring elevated temperatures were conducted with the Pr^{3+}-doped optical fibre in the centre of a Carbolyte (Type 201) tube oven. Due to the thermal gradient within the oven, 100 mm lengths of optical fibre were used in temperature tests, in order to minimise temperature gradients along the active fibre.

During temperature calibrations for the 630 nm wavelength fluorescence peak ($^1D_2 \rightarrow {}^3H_4$), the temperature was raised at a rate of 2 °C per minute, then allowed to settle for 20 minutes before fluorescence lifetime measurements commenced. The temperature difference between readings was 50 °C, from room temperature (≈ 20 °C)

to a maximum temperature of 500 °C. The detection scheme incorporated the PMT with a 40 nm FWHM band pass filter centred around a wavelength of 632 nm in series with the long pass filter.

Calibration for the 870 nm fluorescence peak ($^1D_2 \rightarrow {}^3F_2$, $^3H_6$) used the following procedure: the oven temperature increased by 10 °C at a rate of 1 °C/minute and was left to settle for 15 minutes. This process was used until a temperature of 500 °C was reached. After this, the temperature was incremented by 25 °C and left to settle for 15 minutes as the settling time for the oven at elevated temperatures is quicker than at lower temperatures. A 10 nm FWHM band pass filter centred around 900 nm was used in conjunction with the InGaAs PD to monitor the 870 nm wavelength transition ($^1D_2 \rightarrow {}^3H_4$), as the PMT was unable to detect this transition. For each temperature, ten independent readings were taken before the temperature was increased.

5.4 Strain measurements

Strain measurements for the Pr^{3+}-doped fibres were measured in different conditions. Firstly, the 630 nm wavelength fluorescence lifetime dependence on applied strain was taken with 50 mm lengths of Pr1 and PrAl fibre. The fibre length was 50 mm to ensure that any movement that results from the weights shifting the doped fibre from the centre of the tube oven kept the thermal gradient along the fibre length to a minimum.

The fibres were centred in the tube oven and the temperature was raised to 100 °C and after the tests were completed, the temperature was raised to 200 °C. The resultant fluorescence was filtered with long pass and band pass filters to block the pump wavelength; a PMT measured the fluorescence intensity decay.

Fluorescence lifetime dependence on strain at a fluorescence wavelength of 870 nm used fibre lengths of the order of 700 mm. This was necessary to improve signal-to-noise ratio that was evident in the measurements in the 630 nm wavelength results (section 6.3.1 and 6.3.3). These strain measurements were taken at room temperature because the tube oven could not accommodate such long lengths of fibre. The

fluorescence was detected using an InGaAs detector after a series of filters that blocked the pump light from saturating the detector.

Measurement of these two (630 and 870 nm) fluorescence wavelengths for their strain -fluorescence lifetime characteristics followed the same procedure, in that at the end of the rare-earth fibre, a communications grade fibre was fusion spliced to this fibre, and a clamp was attached that allowed a series of weights to be suspended, thereby resulting the fibre being strained. The clamp provided a minimum strain of 341 με along the fibre and the applied strain was subsequently increased up to 1957 με, through the addition of individual weights, table 5.2 shows the mass of these weights.

Table 5.2 *The mass of the weights used for these strain measurements.*

Mass type	Weight (g)
Clamp	31.9
Weight holder	48.9
Small mass	22.2
Mass 1	49.8
Mass 2	49.9

Each time a weight was added, ten lifetime measurements were taken. This process was reversed, by taking weights off the clamp, until only the clamp remained; this entire process constituted one cycle. Ten cycles were taken during these strain calibrations.

In all measurements, the decay curves were fitted with a least-squares regression computer program (*Table Curve fit v.5*). The strain-fluorescence lifetime results were fitted with the same program to determine the sensitivity of the system.

6 Experimental Analysis

6.1 Chapter Overview

This chapter is separated into three sections; the first two sections discuss the temperature and strain measurements respectively of the $^1D_2$ energy level for both Pr1 (Pr^{3+}-dopant concentration of 700 ppm) and PrAl (Pr^{3+}-dopant concentration of 1000 ppm) silica optical fibres, for the $^1D_2 \rightarrow {}^3F_2$, $^3H_6$ (870 nm) transition, and the $^1D_2 \rightarrow {}^3H_4$ (630 nm) transition. The temperature ranged from 20 to 950 °C, and 20 to 500 °C for the 870 and 630 nm fluorescence transitions, respectively. The applied strain on the fibre ranged from 0 to 1957 με for both Pr^{3+}-doped fibres. The data were analysed using the relevant equations from chapter 4.

The third section discusses the strain dependence for the $^1D_2 \rightarrow {}^3F_2$, $^3H_6$ transition in PrAl fibre, that exhibited an evident strain sensitivity, in terms of the suggestion of Farrell *et al.* [59].

6.2 Temperature measurements

The experimental procedures for temperature measurements for both Pr1 and PrAl-doped fibres were outlined in detail in section 5.3. In short, the Ar^+ laser delivered 100 mW of 488 nm light into a single-mode silica fibre that was fusion spliced (0.01 dB loss) to a doped section (100 mm) of fibre had been centred in a tube oven. Counter-propagating fluorescence intensity decay was detected, by either a PMT or a PD, and the fluorescence intensity decay was fitted using a least squares fitting program (*Table Curve Fit v.5*).

6.2.1 Pr1 fibre from the $^1D_2 \rightarrow {}^3F_2$, $^3H_6$ transition (870 nm)

Figure 6.1 shows the fluorescence lifetime variation as measured from the $^1D_2 \rightarrow {}^3F_2$, $^3H_6$ transition with a photodiode (section 5.2.6) while the Pr1 fibre was slowly heated from 20 to 950 °C. In this figure there are three distinct zones, the first (20 to 500 °C) can be considered as the low temperature zone, where phonon emission has little effect on the fluorescence lifetime and the relationship between fluorescence lifetime and temperature can be approximated to a linear relationship. In the second zone (500 to 800 °C), phonon decay has a significant effect on fluorescent

lifetime, as seen by a dramatic decrease in the fluorescence lifetime. The third zone (800 to 950 °C) where the fluorescence lifetime data deviates from the expected fit.

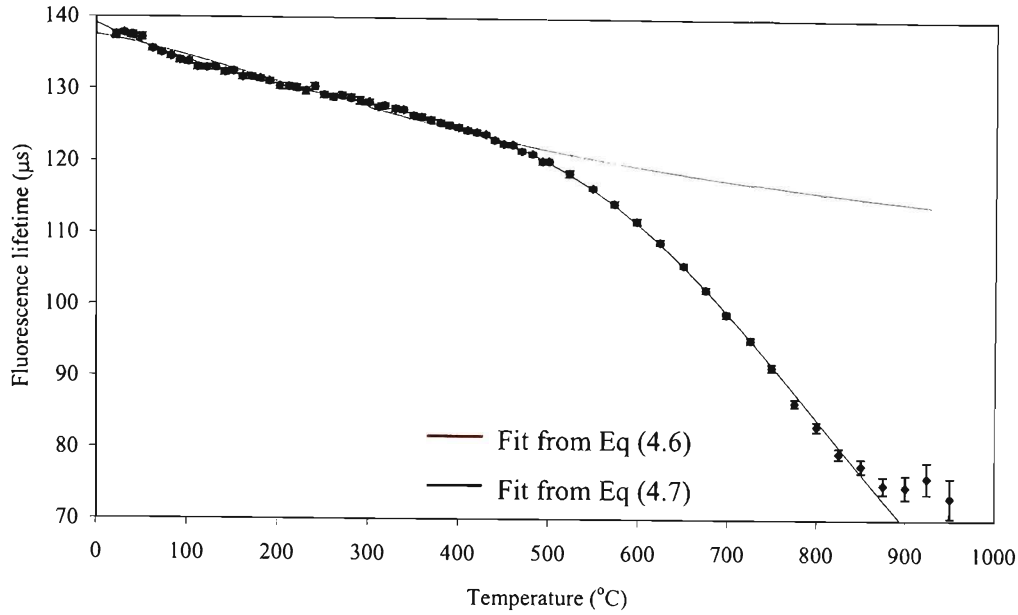

Figure 6.1 *Fluorescence lifetime-temperature graph for Pr1 optical fibre for the* $^1D_2 \rightarrow {}^3F_2, {}^3H_6$ *transition. Data fits from equations 4.6 and 4.7 are shown in red and black, respectively.*

The data points in figure 6.1 were fitted with equations 4.6 and 4.7 (i.e. phonon effects included) over a temperature range from 20 to 500 °C and 20 to 700 °C, respectively, to determine how the energy level width and transition rate parameters are affected by different equations over different ranges. The temperature sensitivity over the temperature range 0 to 500 °C for this fibre was measured as –33 ± 1 ns/°C (assuming a linear fit) and the fitting parameters used in equations 4.6 and 4.7 are shown in table 6.1.

Table 6.1 *Parameters used to fit fluorescence lifetime-temperature measurements in Pr1 optical fibre.*

Equation.	**Temperature range (°C)**	**ΔE (cm^{-1})**	**w_{10} (s^{-1}) ($\times 10^3$)**	**w_{20} (s^{-1}) ($\times 10^3$)**	**ΔE_q (cm^{-1})**	**w_q (s^{-1}) ($\times 10^6$)**
4.6	20 → 500	830 ± 50	7.20 ± 0.03	13.0 ± 0.4		
4.7*	20 → 700	340 ± 50	6.6 ± 0.2	10.5 ± 0.1	4300 ± 100	3.2 ± 0.5

* Phonon effects included.

The results in table 6.1 indicate that the energy level separation (ΔE) parameter changes significantly, whereas the transition rates are not significantly changed in either case. Equation 4.7 produced a realistic value for ΔE for the $^1D_2$ energy level to fit the data; inspection of figure 3.4 shows that the $^1D_2$ energy level is less likely to be 833 cm^{-1}. Correspondingly, the value for ΔE_q and τ_q is within reasonable agreement with fluorescence lifetime measurements for Yb^{3+}-doped silica optical fibres [70].

6.2.2 Pr1 fibre from the $^1D_2 \rightarrow {}^3H_4$ transition (630 nm)

The fluorescence lifetime was taken for the $^1D_2 \rightarrow {}^3H_4$ transition of the Pr1 fibre, over a temperature range from 20 to 500 °C. The fluorescence lifetime measurements were taken to determine the temperature sensitivity over this range, the results of which are shown in figure 6.2.

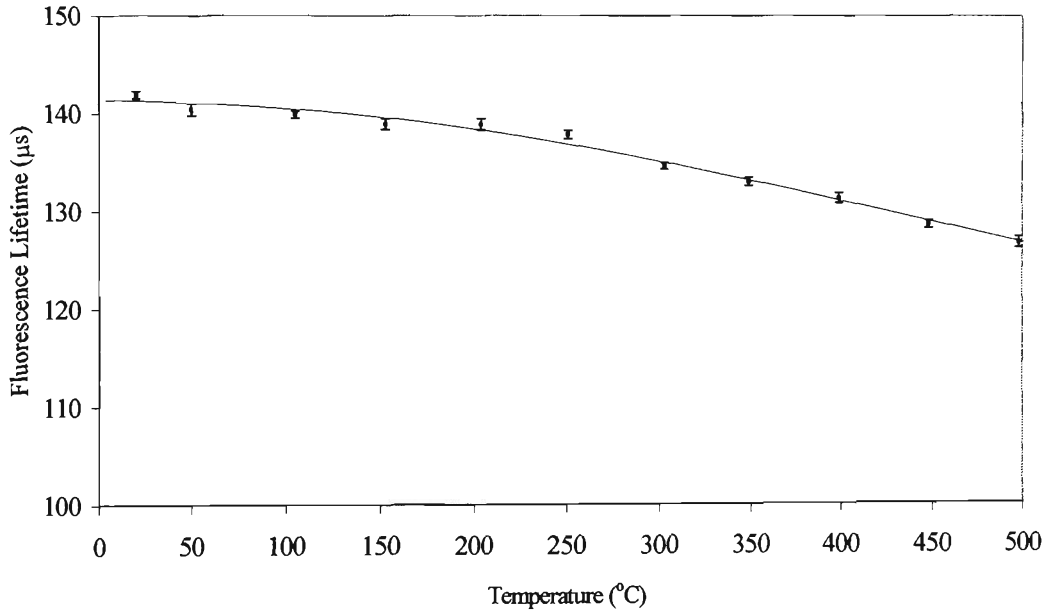

Figure 6.2 *Fluorescence lifetime measurements of Pr1 fibre over a temperature range from 20 to 500 °C, for the $^1D_2 \rightarrow {}^3H_4$ transition.*

Fluorescence lifetime data for the $^1D_2 \rightarrow {}^3H_4$ transition was measured using a PMT and fitted with equation 4.6 since no significant phonon emission is evident. The parameters required to fit the data in figure 6.2 are shown in table 6.2 and the temperature sensitivity was determined to be -30 ± 2 ns/°C over this temperature range, assuming a linear fit.

Table 6.2 *Parameters used to fit data in figure 6.2*

Temperature range (°C)	ΔE (cm^{-1})	w_{10} (s^{-1}) ($\times 10^3$)	w_{20} (μs^{-1}) ($\times 10^3$)
20 → 500	1500 ± 100	7.06 ± 0.01	19.2 ± 0.4

These results have similar transition rates when compared to the parameters in table 6.1; this is expected as these fluorescence lifetime measurements originate from the same energy level. The value for ΔE is unrealistic as it is too large for the $^1D_2$ level.

6.2.3 PrAl fibre from the $^1D_2 \rightarrow {}^3F_2, {}^3H_6$ transition (870 nm)

The fluorescence lifetime dependence for the $^1D_2 \rightarrow {}^3F_2, {}^3H_6$ transition, having a fluorescence peak centred at a wavelength of 870 nm was measured over a temperature range from 20 to 950 °C and is shown in figure 6.3.

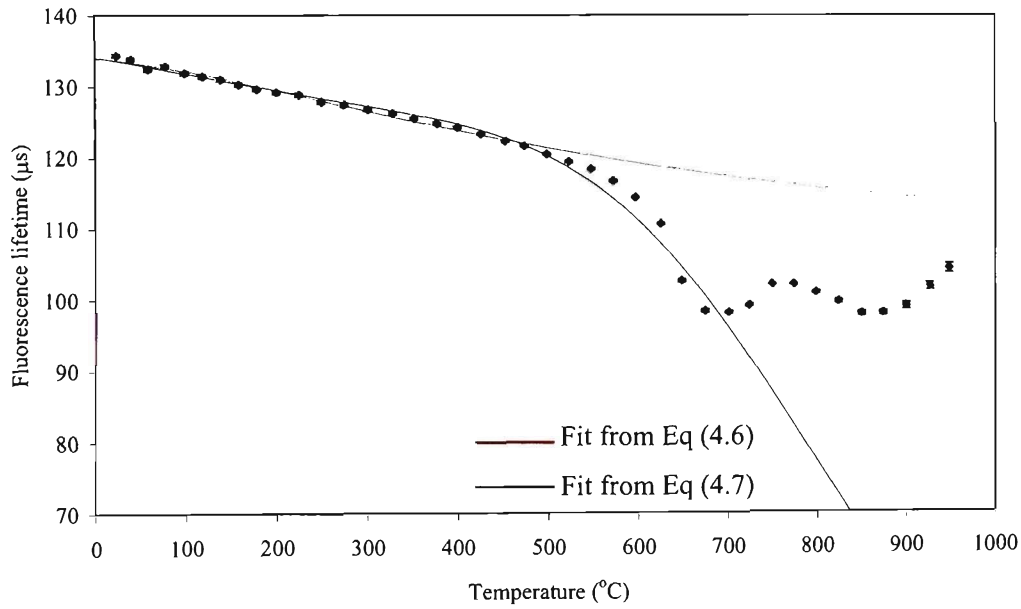

Figure 6.3 *Fluorescence lifetime-temperature graph for PrAl optical fibre for the $^1D_2 \rightarrow {}^3F_2, {}^3H_6$ transition. Data fits from equations 4.6 and 4.7 are shown in red and black, respectively.*

The data points in figure 6.3 were fitted with equations 4.6 and 4.7 over a temperature range from 20 to 500 °C and 20 to 700 °C, respectively. These equations were fitted to the fluorescence lifetime data to determine how the energy level width and transition rate parameters are affected by different equations over different ranges. The temperature sensitivity over the temperature range from 0 to 500 °C for this fibre was determined to be ≈ –20 ± 6 ns/°C, assuming a linear fit, and the fitting parameters used in equations 4.6 and 4.7 are shown in table 6.3.

Table 6.3 *Parameters used to fit equations 4.6 and 4.7 in figure 6.3*

Equation	Temperature range (°C)	ΔE (cm^{-1})	w_{10} $(s)^{-1}$ $(\times 10^3)$	w_{20} $(s)^{-1}$ $(\times 10^3)$	ΔE_q (cm^{-1})	w_q $(s)^{-1}$ $(\times 10^6)$
4.6	20 → 500	930 ± 60	7.43 ± 0.02	12.8 ± 0.5		
4.7*	20 → 700	670 ± 300	7.1 ± 0.5	10.1 ± 0.5	5000 ± 700	7.2 ± 0.1

* Phonon effects included.

From table 6.3, the ΔE value from equation 4.6 appears to be unrealistic because the value is too large. The ΔE value that was used in equation 4.7 has a significant uncertainty that may be due to a lower number of readings taken at higher temperatures.

6.2.4 PrAl fibre from the $^1D_2 \rightarrow {}^3H_4$ transition (630 nm)

The fluorescence lifetime was measured for the $^1D_2 \rightarrow {}^3H_4$ transition of the PrAl fibre, over a temperature range from 20 to 500 °C. The fluorescence lifetime measurements were taken to determine the temperature sensitivity over this range, the results of which are shown in figure 6.4.

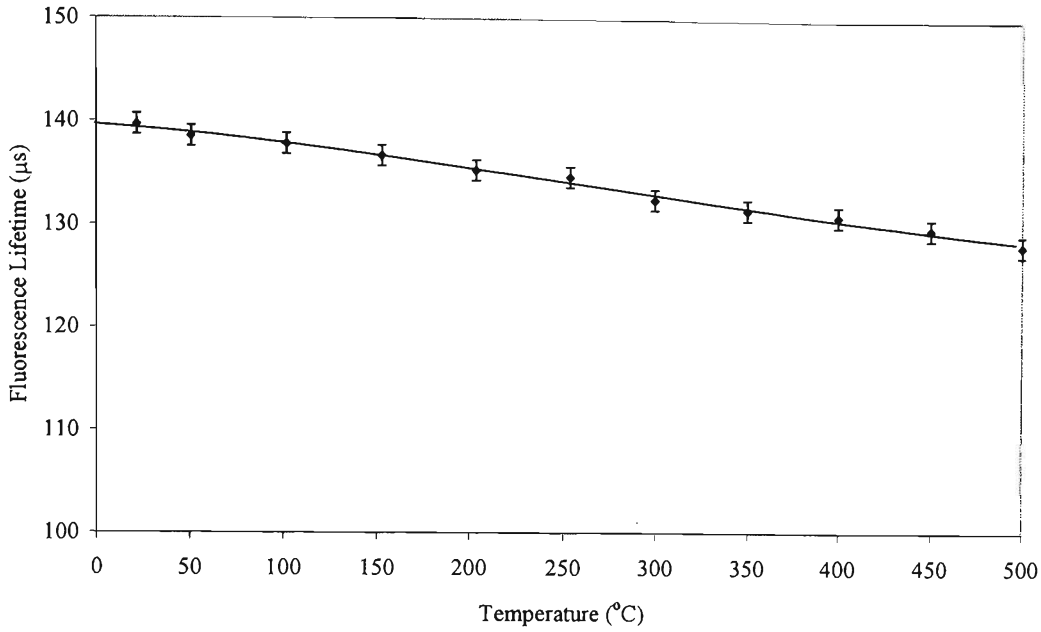

Figure 6.4 *Fluorescence lifetime measurements of Pr1 fibre over a temperature range from 20 to 500 °C for the $^1D_2 \rightarrow {}^3H_4$ transition.*

Fluorescence lifetime data for the $^1D_2 \rightarrow {}^3H_4$ transition were measured using a PMT and fitted with equation 4.6 (p. 4-9) since no significant phonon emission is evident. The parameters required to fit the data in figure 6.4 are shown in table 6.4 and the temperature sensitivity were found to be -20 ± 4 ns/°C over this temperature range, assuming a linear fit.

Table 6.4 *Parameters used to fit data in figure 6.4*

Temperature range (°C)	**ΔE (cm^{-1})**	**w_{10} $(s)^{-1}$ $(\times 10^3)$**	**w_{20} $(s)^{-1}$ $(\times 10^3)$**
20 → 500	930 ± 80	7.13 ± 0.03	11.3 ± 0.5

The energy level width in table 6.4 seems too large for the $^1D_2$ energy level, while the transition rates, however, are similar to the rates for the $^1D_2 \rightarrow {}^3F_2$, $^3H_6$ transition.

6.3 Strain measurements

Strain measurement techniques for both Prl and PrAl-doped fibres have already been outlined in detail (section 5.4). As for the temperature measurements, the Ar^{+} laser (488 nm) delivered 100 mW into a single-mode silica fibre that was fusion spliced to a length of Prl optical fibre, centred in a tube oven. A single mode telecommunications grade optical fibre was spliced on the other end of the Pr^{3+}-doped fibre, where weights would be attached to produce strain along the length of the fibre. Counter-propagating fluorescence intensity decay was detected, and the resultant decay curve was fitted.

The Pr^{3+}-doped optical fibre for strain measurements at elevated temperatures had a length of 50 mm to ensure that in the event of the fibre moving between measurements that the temperature gradient along the fibre's length was minimal. The $^{1}D_2 \rightarrow {}^{3}H_4$ transition that fluoresced with a central wavelength of 630 nm was measured for these strain measurements.

The length of the Pr^{3+}-doped optical fibre was increased to 700 mm during strain measurements at room temperature, to ensure better signal to noise ratios. The $^{1}D_2 \rightarrow {}^{3}F_2, {}^{3}H_6$ transition fluorescing at wavelengths centred at 870 nm was measured for these strain measurements.

6.3.1 Pr1 fibre from the $^1D_2 \rightarrow {}^3H_4$ transition (630 nm)

Figure 6.5 shows the fluorescence lifetime variation from the $^1D_2 \rightarrow {}^3H_4$ transition from a 50 mm length of Pr1 fibre centred in the tube oven at elevated temperatures. The fitted fluorescence lifetime-strain sensitivities from the data in figure 6.5, are $(0 \pm 30) \times 10^{-5}$ μs/με and $(10 \pm 10) \times 10^{-5}$ μs/με at 100 and 200 °C, respectively.

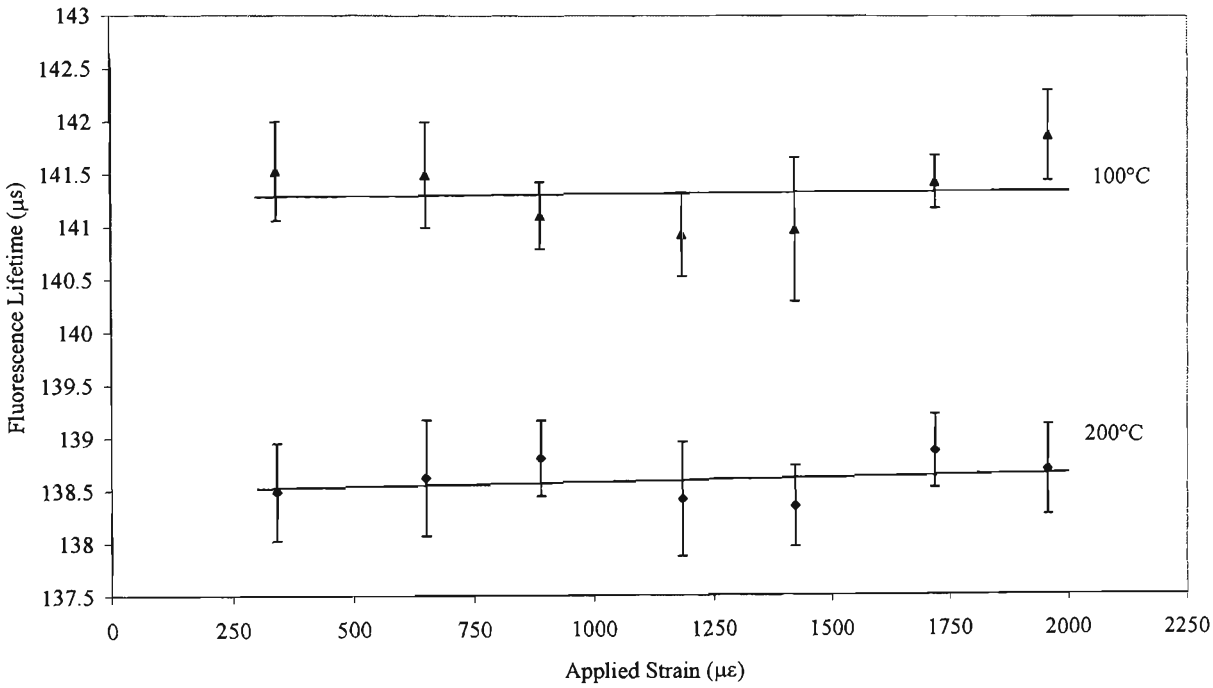

Figure 6.5 *The fluorescence lifetime for the $^1D_2 \rightarrow {}^3H_4$ transition with respect to strain for a Pr1 fibre, with a length of 50 mm at 100 and 200 °C.*

The error bars in figure 6.5 are the result of very low fluorescence intensities from the short (50 mm) length of Pr1 fibre, as well as a low signal-to-noise ratio associated with the PMT detecting these weak signals. From the data shown in figure 6.5, no conclusion concerning the overall strain dependence of lifetime can be reached.

6.3.2 Pr1 fibre from the $^1D_2 \rightarrow {}^3F_2, {}^3H_6$ transition (870 nm)

Figure 6.6 shows the fluorescence lifetime variation from the $^1D_2 \rightarrow {}^3F_2, {}^3H_6$ transition from a 700 mm length of Pr1 fibre at room temperature (24.9 ± 0.1 °C). The fitted fluorescence lifetime-strain sensitivity from the data in figure 6.6, is $(-2 \pm 1) \times 10^{-5}$ μs/με.

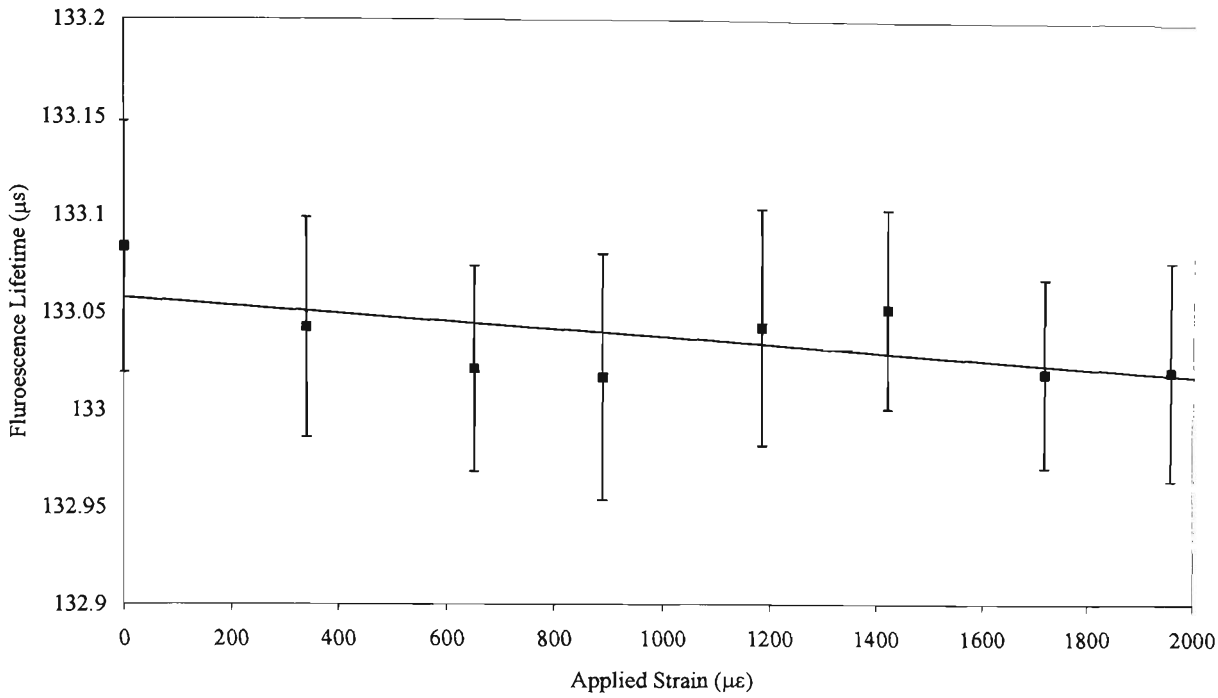

Figure 6.6 *The fluorescence lifetime variation for the $^1D_2 \rightarrow {}^3F_2$, $^3H_6$ transition with respect to applied strain for Pr1 fibre at room temperature.*

The error bars in figure 6.6 are much smaller than those in figure 6.5, due to an increase in fluorescence intensity caused by the use of a longer length of Pr1 fibre (i.e. 700 mm instead of 50 mm). The error bars have decreased by 90% from the error bars in figure 6.5. The fluorescence lifetime-strain measurements appear to have a decreasing relationship, i.e. a slightly negative gradient.

6.3.3 PrAl fibre from the $^1D_2 \rightarrow {}^3H_4$ transition (630 nm)

Figure 6.7 shows the fluorescence lifetime variation from the $^1D_2 \rightarrow {}^3H_4$ transition from a 50 mm length of PrAl fibre centred in a tube oven at elevated temperature. The fluorescence lifetime-strain sensitivities from the data in figures 6.7 are, $(10 \pm 20) \times 10^{-5}$ and $(0 \pm 20) \times 10^{-5}$ μs/με at 100 and 200 °C, respectively.

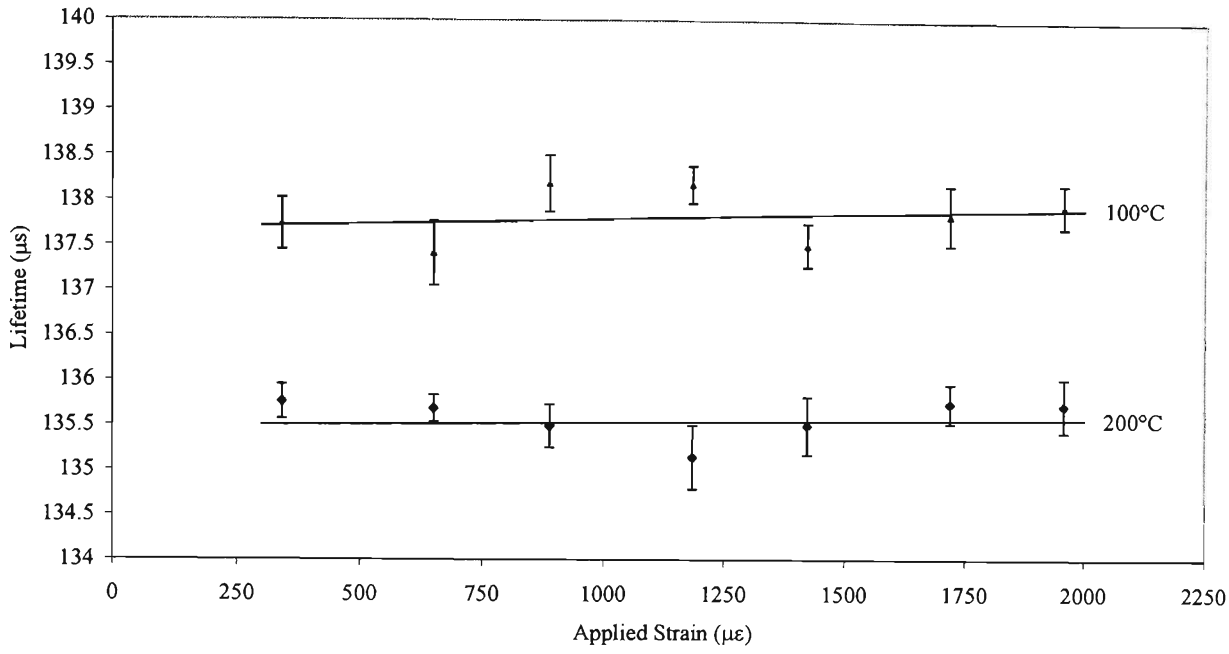

Figure 6.7 *Lifetime variation of strain between 341 and 1957 με. These measurements were taken at temperatures of 100 and 200 °C from the $^1D_2 \rightarrow {}^3H_4$ transition in Pr1 fibre at a length of 50 mm.*

Figure 6.7 does not determine conclusively the strain sensitivity of the PrAl optical fibre, because the error bars and the scatter of the data are large. However, as the Pr^{3+} concentration in PrAl fibre is higher than that of Pr1 fibre the error bars are reduced due to higher fluorescence intensity.

6.3.4 PrAl fibre from the $^1D_2 \rightarrow {}^3F_2, {}^3H_6$ transition (870 nm)

Figure 6.8 shows the fluorescence lifetime variation from the $^1D_2 \rightarrow {}^3F_2, {}^3H_6$ transition from a 700 mm length of PrAl fibre at room temperature (24.9 ± 0.1 °C) under strain as measured with a photodiode. The fitted fluorescence lifetime-strain sensitivities from the data in figure 6.8, is $(-5.6 \pm 0.6) \times 10^{-5}$ μs/με, over the full strain range (0 to 1957 με).

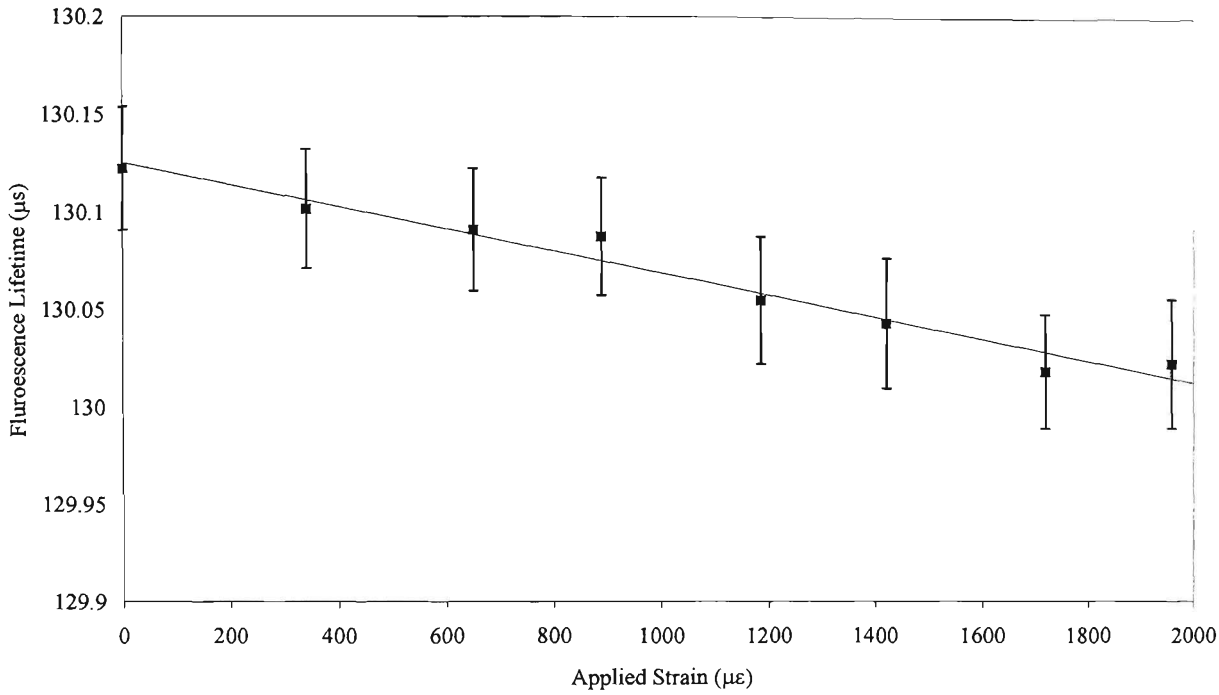

Figure 6.8 *Lifetime variation of strain between 341 and 1957 με. These measurements were taken at room temperature with a 700 mm length of PrAl fibre from the* $^1D_2 \rightarrow {}^3F_2, {}^3H_6$ *transition.*

The error bars in figure 6.8 have been reduced significantly compared with those in figure 6.7, is due to an increase in the signal-to-noise ratio as a consequence to an increase in fibre length. One possible reason that causes the decreasing fluorescence lifetime with an increase of applied strain will be discussed in the next section.

6.4 Strain sensitivity of PrAl fibre $^1D_2 \rightarrow {}^3F_2, {}^3H_6$ transition

In the previous section the strain sensitivity from the $^1D_2 \rightarrow {}^3F_2, {}^3H_6$ transition in PrAl fibre exhibited a definite negative fluorescence lifetime-strain trend. This was unexpected as the trends from other rare-earth-doped materials display a positive trend [26]. In order to further understand this process equation 4.21 was used. This equation gives fluorescence lifetime as a function of transition rates and energy level separation assuming these all have possible strain dependence. The effect of strain on the transition rates w_{10} and w_{20} in equation 4.21 are shown in figure 6.9.

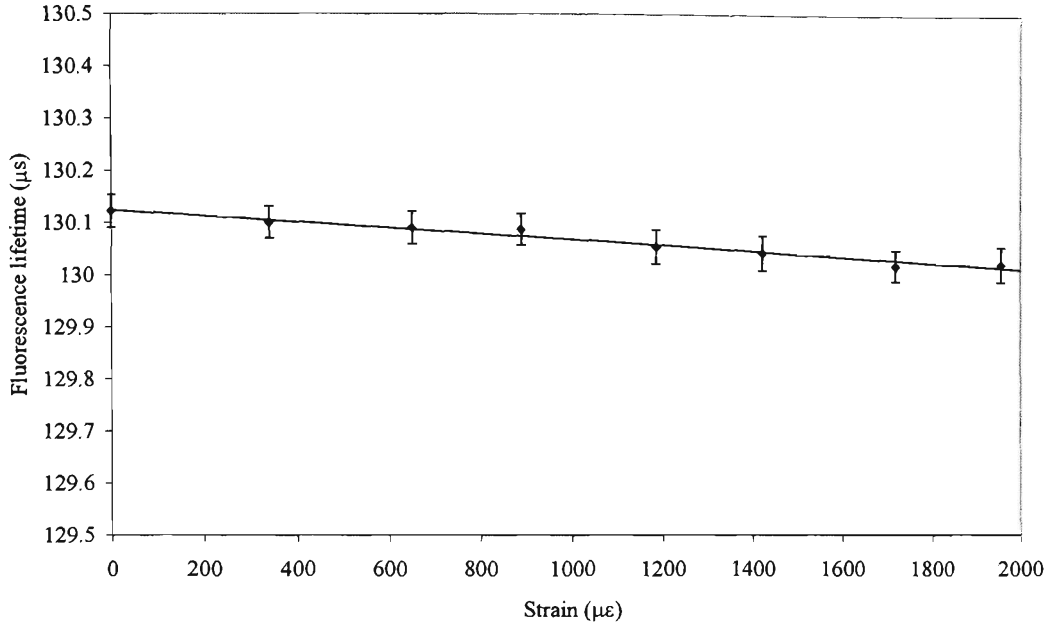

Figure 6.9 *The effect of strain on the radiative fluorescence rates w_{10} and w_{20} from the $^1D_2$ level in PrAl fibre from the $^1D_2 \rightarrow {}^3F_2, {}^3H_6$ transition.*

The strain coefficients k_{10} and k_{20} used had values of (0 ± 300) $s^{-1}\mu\varepsilon^{-1}$ and (–0 ± 2000) $s^{-1}\mu\varepsilon^{-1}$, respectively. The transition rates have a good fit but high parameter uncertainty. This indicates that the method used to measure fluorescence lifetime-based strain measurements are required to have greater precision in order to use Farrell *et al*'s theory [59]; to describe the physical origin of strain for fluorescence lifetime-strain dependency. The photo-detectors used to take these measurements require higher fluorescence intensity from the Pr^{3+}-doped fibre to increase the accuracy of the lifetime measurements.

When ΔE is assumed strain sensitive (with w_{10} and w_{20} strain independent) the fluorescence lifetime–strain fit is shown in figure 6.10.

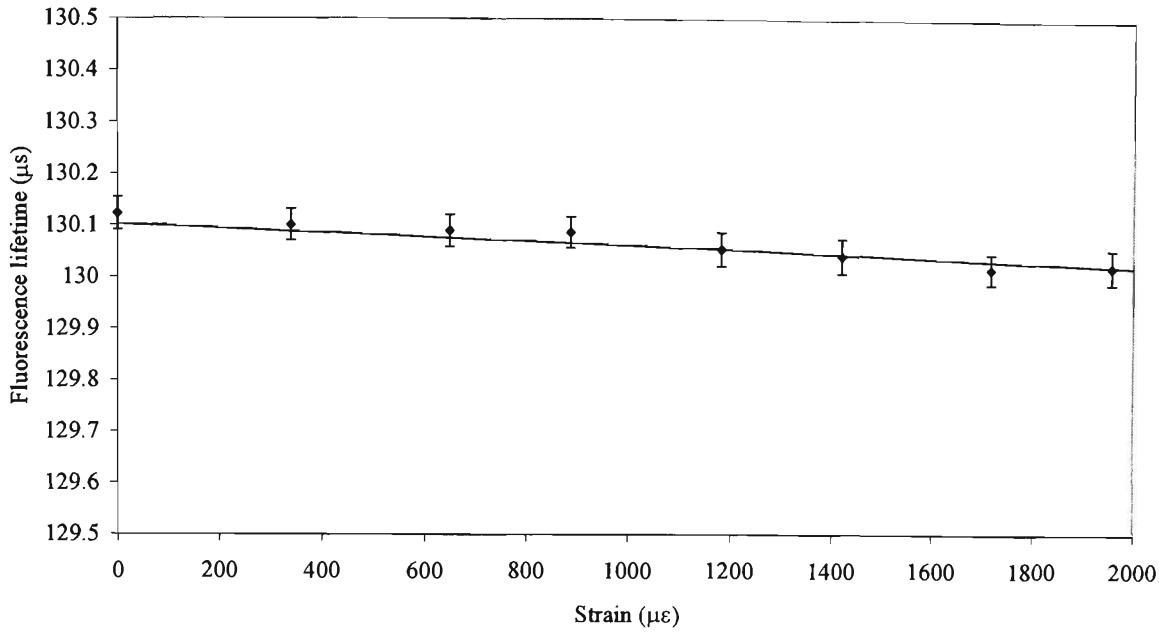

Figure 6.10 *Fluorescence lifetime-strain fitting to the PrAl from the $^1D_2 \rightarrow {}^3F_2, {}^3H_6$ transition when ΔE is assumed strain dependent.*

The data in figure 6.10 were fitted with ΔE strain coefficient, *b*, (equation 4.19), equal to $(8 \pm 1) \times 10^{-6}$ $cm^{-1}\mu\varepsilon^{-1}$. This strain sensitivity corresponds to a 1 pm shift in the 890 nm fluorescence wavelength when strained with 1000 με. The effect of strain on ΔE is negligible as predicted in section 4.7.

6.5 Conclusion

Measurement of the temperature and strain characteristics of Pr1 and PrAl silica optical fibres has been carried out over a temperature range from 20 to 950 °C, and strain measurements over a range from 0 to 1957 με at various temperatures.

The fluorescence lifetime-temperature sensitivity over a temperature range from 20 to 500 °C from the Pr1 and PrAl fibres was measured as (-30 ± 2) ns/°C and (-20 ± 4) ns/°C, respectively. At temperatures above 500 °C, phonon emission was pronounced in both fibres as fluorescence lifetime decreased rapidly as expected.

Fluorescence lifetime-strain measurements showed interesting results. Measurements from both fibres at elevated temperature had a low signal-to-noise ratio, due to weak fluorescence levels. At room temperature, both fibres had higher signal-to-noise ratio levels. Unfortunately, strain measurements from the Pr1 fibre were inconclusive as to

the extent of its strain sensitivity. Strain measurements from the PrAl fibre indicate a clear negative trend in fluorescence lifetime with increasing strain. However, the results were not sufficiently precise to determine accurately the physical processes that are taking place that allow this behaviour.

7 Summary and discussion of measurements

7.1 Chapter overview

This chapter provides a summary of the measurements reported in the previous chapter. Comparison is made between the measurements for the two Pr^{3+}-doped silica optical fibres investigated in this thesis and results for Nd^{3+}, Er^{3+} and Yb^{3+} -doped optical silica fibres reported previously.

7.2 Comparison between Pr1 and PrAl fibres

7.2.1 Temperature measurement comparison

Although the Pr1 and PrAl fibres are inherently different, both in Pr^{3+}-dopant levels and in Al^{3+} concentration levels, it is of interest to compare the fluorescence lifetime fit parameters for temperature measurements for Pr1 and PrAl optical fibres, from section 6.2 in table 7.1.

Table 7.1 *The parameters obtained for Pr1 and PrAl fibres to determine the temperature dependence of fluorescence lifetime.*

Fibre	Temperature Range (°C)	Central Wavelength (nm)	ΔE (cm^{-1})	w_{10} (s^{-1}) ($\times 10^3$)	w_{20} (s^{-1}) ($\times 10^3$)	ΔE_q (cm^{-1}) ($\times 10^3$)	w_q (s^{-1}) ($\times 10^6$)	Eq.
Pr1	20 → 500	630	1500 ± 100	7.06 ± 0.01	19.2 ± 0.4			4.6
Pr1	20 → 500	870	830 ± 50	7.20 ± 0.03	13.0 ± 0.4			4.6
Pr1	20 → 700	870	340 ± 50	6.6 ± 0.2	10.5 ± 0.1	4.3 ± 0.1	3.2 ± 0.5	4.7
PrAl	20 → 500	630	930 ± 80	7.13 ± 0.03	11.3 ± 0.5			4.6
PrAl	20 → 500	870	930 ± 60	7.43± 0.02	12.8 ± 0.5			4.6
PrAl	20 → 700	870	670 ± 300	7.1 ± 0.5	10.1 ± 0.5	5.0 ± 0.7	7.2 ± 0.1	4.7

The transitions in each of the measurements in table 7.1 originate from the same energy level, so their transition rates and energy level spacing (ΔE) for each fibre should be similar, if not the same. The results show that there is good correlation of the w_{10} and w_{20} rates between each set of measurements for both Pr1 and PrAl fibres. Pr1 has more spread in values than the PrAl fibre; this can be attributed to lower signal to noise ratio during measurements from the Pr1 fibre as there was less fluorescence intensity than from the PrAl fibre.

The energy level spacing parameter from the PrAl fibre over the 0 to 500 °C range, are identical and have low uncertainties. This is most likely caused by low scatter of

fluorescence lifetime measurements over temperatures ranging from 0 to 500 °C. The value of ΔE from the measurement from PrAl fibre over the temperature range from 20 to 700 °C has decreased substantially (≈ 30% reduction) to 670 cm^{-1}. This decreased value makes more sense than the other two ΔE values because a separation in the order of 1000 cm^{-1} is significant and is comparable to the thermalised energy levels that are common to other rare-earths. The $^1D_2$ energy level separation should be in the order of several 100 cm^{-1}. Similarly, the ΔE values for the Pr1 fibre over both temperature ranges should also be approximately several 100 cm^{-1} wide. One reason why the ΔE value is low for both Pr1 and PrAl fibres over the temperature range from 0 to 700 °C is an increase in the separation between the temperature measurements, that, with also an increase in their error bars may lead to higher error in the fitting parameters. The parameters ΔE_q and w_q for both Pr1 and PrAl fibres are in the same order of magnitude as those obtained for Yb^{3+}-doped fibre [70].

The temperature sensitivities for both Pr1 and PrAl fibres are shown in table 7.2 over the temperature range from 0 to 500 °C. The relative temperature sensitivity (%/°C), provides a convenient means of comparing the temperature sensitivity between materials. This parameter was determined by dividing the temperature sensitivity of the fibre by a datum along the fit, and then converting to a percentage. As the temperature measurements are from the same energy level, their temperature sensitivities should be very similar.

Table 7.2 *The temperature sensitivity for the Pr1 and PrAl optical fibres over a temperature range from 0 to 500 °C.*

Fibre	Central wavelength (nm)	Temperature sensitivity (ns/°C)	Relative temperature sensitivity (%/°C)
Pr1	630	-(30 ± 2)	-0.020 ± 0.002
Pr1	870	-(33 ± 1)	-0.030 ± 0.004
PrAl	630	-(20 ± 4)	-0.010 ± 0.004
PrAl	870	-(20 ± 6)	-0.020 ± 0.003

The temperature sensitivities from the Pr1 fibre are very similar, because their fluorescence transition originates from the same energy level. Likewise, the same can be said about the temperature sensitivity of the PrAl fibre.

7.2.2 Strain measurement comparison

The parameters used to fit the fluorescence lifetime-strain measurements with a straight line for Pr1 and PrAl fibres are shown in table 7.3. The relative strain sensitivities (%/με) provide a convenient means of comparing the strain sensitivity between materials. This parameter was determined by dividing the strain sensitivity of the fibre by a datum along the fit, and then converting to a percentage.

The results are from measurements taken at room temperature for both Pr1 and PrAl optical fibres; the length of the optical fibres were 700 mm. Measurements were taken from the $^1D_2 \rightarrow {}^3F_2, {}^3H_6$ transition.

Table 7.3 *Strain sensitivity of Pr1 and PrAl optical fibres over a strain range from 0 to 1957 με.*

Fibre	Fluorescence wavelength (nm)	Strain sensitivity (μs/με) ($\times 10^{-5}$)	Relative strain sensitivity (%/με) ($\times 10^{-5}$)
Pr1	870	-2 ± 1	-1.5 ± 0.8
PrAl	870	-5.6 ± 0.6	-4.3 ± 0.5

The strain sensitivities of these two fibres are within the same order of magnitude. The large errors associated with these measurements are caused by the small effect that strain has on fluorescence lifetime from rare-earth-doped optical fibres.

7.3 Comparison with other rare-earth-doped optical fibres

Measurements of the effect of temperature and strain have on the fluorescence lifetime from different rare-earth-doped silica optical fibres have been conducted by various authors. These are shown in table 7.4, along with the measurements from this thesis. The relative strain-temperature cross-sensitivity was determined using equation 4.11; this quantity is a convenient method to determine how applied strain or temperature effects can alter the temperature or strain measurements.

Table 7.4 *Comparing the values of ΔE, strain sensitivity, temperature sensitivity and strain-temperature cross-sensitivity in various rare-earth-doped optical fibres with fluorescence lifetime-based sensing.*

Fibre type	ΔE (cm^{-1})	Strain sensitivity (%/με) ($\times10^{-5}$)	Temperature sensitivity (%/°C)	Strain-temperature cross-sensitivity (°C/με)	Ref.
(700 ppm Pr^{3+})	340	(-1.5 ± 0.8)	-0.030 ± 0.002	(0.5 ± 0.3) $\times10^{-3}$	[This work]
(1000 ppm Pr^{3+})	670	(-4.3 ± 0.5)	-0.020 ± 0.003	(2.2 ± 0.8) $\times10^{-3}$	[This work]
(2.5% Yb^{3+})	680	(4.9 ± 0.9)	-0.008 ± 0.001	(-6 ± 1) $\times10^{-3}$	[26]
(250 ppm Nd^{3+})	1000	(1.1 ± 0.2)	-0.0594 ± 0.0007	(-1.9 ± 0.3) $\times10^{-3}$	[61]
(990 ppm Nd^{3+})	1000	(9.7 ± 3.8)	-0.0348 ± 0.0001	(-2.8 ± 1.2) $\times10^{-3}$	[61]
(1460 ppm Nd^{3+})	1000	(7.1 ± 3.6)	-0.0441 ± 0.0001	(-1.6 ± 0.8) $\times10^{-3}$	[61]
(4000 ppm Nd^{3+})	1000	(9.8 ± 2.6)	-0.0617 ± 0.0001	(-1.6 ± 0.5) $\times10^{-3}$	[61]
(200 ppm Er^{3+})	1000	(9.7 ± 1.9)	-0.024 ± 0.002	(-4.0 ± 1.1) $\times10^{-3}$	[26]
(960 ppm Er^{3+})	1000	(11.9 ± 3.0)	-0.025 ± 0.003	(-4.7 ± 1.0) $\times10^{-3}$	[26]
(4370 ppm Er^{3+})	1000	(8.66 ± 2.0)	-0.017 ± 0.001	(-5.2 ± 1.3) $\times10^{-3}$	[71]

Table 7.4 shows for all of the rare-earth-doped optical fibres investigated to date, the strain and temperature sensitivities of fluorescence lifetime are similar. However, Pr^{3+}-doped optical fibres have temperature sensitivities similar to that of other rare-earth-doped optical fibres, but strain sensitivity has the opposite sign. Nevertheless the magnitude of this strain sensitivity is effectively the same for PrAl fibre, and slightly smaller for the Pr1 fibre. It is uncertain if the strain sensitivity is

concentration dependent and the effect of Al^{3+} concentration within the fibre for temperature or strain sensitivity is unclear. The strain-temperature cross-sensitivity of the rare-earth-doped optical fibres in table 7.4 is shown graphically in figure 7.1 as a function of concentration

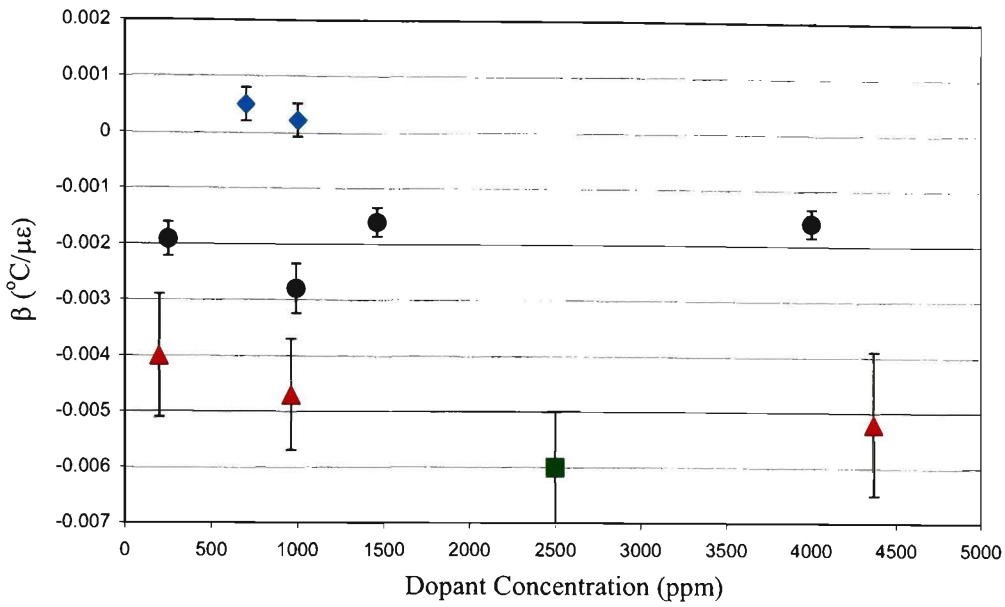

Figure 7.1 *Strain-temperature cross-sensitivity (β) for; Pr^{3+}-(diamond), Nd^{3+}-(circle), Er^{3+}-(triangle), Yb^{3+}-(square) -doped silica optical fibres.*

Figure 7.1 illustrates how the strain-temperature cross-sensitivities of Nd^{3+}, Er^{3+} and Yb^{3+} –doped silica optical fibres are all negative, whilst the Pr^{3+}-doped silica fibres display a positive strain-temperature cross-sensitivity. The model of Farrell *et al.* [59] can account for the negative values in the cases of where cross-relaxation processes (section 4.5.2) occur; the application of strain is believed to reduce the concentration slightly, resulting in an increase on fluorescence lifetime. It is not apparent how their model would apply to Yb^{3+}, which has just a single level. A model of this nature, however, cannot account for the new data presented here.

The energy level separation (ΔE) for the rare-earth-doped optical fibres listed are all very similar, except for both Pr^{3+} and Yb^{3+}-doped optical fibres. The reason why Nd^{3+} and Er^{+3}-dopants have a large energy separation is that they use a pair of thermalised energy levels. An advantage in using a pair of energy levels is that the energy level separation is generally larger and this results in a higher temperature sensitivity, than that of single energy levels that have several Stark levels within its structure. Examples of this are the solitary $^2F_{5/2}$ energy level in Yb^{3+} ions and the $^1D_2$ energy

level in Pr^{3+} ions, both of which have ΔE values in the order of 100s of cm^{-1}; consequently, their temperature sensitivity is generally less than that of the other rare-earth ions, but their strain sensitivities are similar.

7.4 Conclusion

A comparison between the two transitions in each of Pr1 and PrAl fibres has been conducted. The w_{10} and w_{20} transition rates for both fibres are similar for both fibres, but their energy level separation vary dramatically.

The temperature and strain sensitivity within the Pr1 and PrAl fibres were similar as the fluorescence transition originated from the same energy level for both fibres. When comparing the PrAl and Pr1 optical fibres to other rare-earth ions, only the Pr^{3+}-doped fibre has negative strain sensitivity co-efficient.

8 Conclusion

8.1 Conclusion

The fluorescence lifetime for Pr^{3+}-doped silica optical fibres has been investigated over a temperature range from 20 to 700 °C and a strain range from 0 to 1957 με. The Pr^{3+} concentration was 700 and 1000 ppm namely, for the fibres denoted Pr1 and PrAl respectively, the latter of which had an Al^{3+}-dopant concentration of 4000 ppm.

The fluorescence lifetime-temperature sensitivity was determined ≈ 30 ns/°C and 20 ns/°C for Pr1 and PrAl fibres respectively. This was found to be similar to the temperature sensitivity from other rare-earth-doped optical fibres. Additionally, the *magnitude* for the strain sensitivity for these two fibres was found to be approximately the same for that of other rare-earth-doped optical fibres, $-(2 \pm 1)\times 10^{-5}$ μs/με and $-(6 \pm 1)\times 10^{-5}$ μs/με for Pr1 and PrAl fibres, respectively.

The strain sensitivity from the PrAl fibre was found to have a negative slope for increasing strain from the $^1D_2 \rightarrow {}^3F_2$, $^3H_6$ transition, which is different from the strain sensitivity of Nd^{3+}, Er^{3+} and Yb^{3+}-doped silica optical fibres. The origin of the strain sensitivity of fluorescence is yet to be fully understood. Whilst the model of Farrell *et al.* [59] describes some data adequately, it does not account for the new measurements presented here (for Pr^{3+}) or data from fluorescence intensity ratio data.

The results indicate that the fluorescence lifetime-strain dependence from the $^1D_2$ energy level in Pr^{3+}-ion behaves differently to that of the Yb^{3+}-ion, even though the energy levels investigated are both single lines split into several Stark levels.

More research is required to understand the processes that make fluorescence lifetime measurements strain sensitive. Understanding of these effects will allow the design of fluorescence lifetime –based temperature and strain sensors, or sensors with particular sensitivities.

8.2 Future Research

This work can be further refined and extended in the following ways. Firstly, the pump wavelength should be resonant to that of the $^1D_2$ energy level ($\approx$ 590 nm). An increase in the fluorescence intensities would improve signal to noise of the photo-detectors.

Additionally, more Pr^{3+}-doped fibres could be manufactured at the *Laboratorie de Physique de la Materière Condensé, Université de Nice*, France, where the Pr1 and PrAl fibres were created. Indeed more fibres in all the rare-earths are needed to obtain consistent data sets (eg. in figure 7.1 one cannot assume that all the Nd^{3+}-doped fibres are made of the same material). These new fibres would have different Pr^{3+}-dopant concentrations in both silica and silica with different Al^{3+}-dopant concentrations. This would help determine how Pr^{3+} and Al^{3+} concentrations affect the strain sensitivity of these fibres from the $^1D_2$ energy level.

Measurements could also be made for Pr^{3+}-doped fluorozirconate fibres, to determine how the ^3P, $^1D_2$ and $^1G_4$ energy levels are affected by strain. This would help investigators determine the extent that outside influences have on individual energy levels. Again, different Pr^{3+}-dopant concentrations can be used to determine its effect on fluorescence lifetime–strain dependence. Fluoride fibres can be doped with higher rare-earth concentrations than that of silica fibres, thereby increasing the fluorescence intensity.

Studies can also be made to determine the oscillator strength of transitions originating from the $^1D_2$ energy. Oscillator strength can be used to determine how effective an actual radiative transition compares to that of an ideal system. Most materials have an oscillator strength that is between zero and one, as transitions are usually not ideal oscillators, although there are some transitions that have an oscillator strength greater than one [72]. These measurements will help further understanding in the spectroscopic nature of Pr^{3+}-doped silica fibre that will allow the development of better performance in optical applications.

References

[1] K.T.V. Grattan and Z.Y. Zhang, *Fiber Optic Fluorescence Thermometry*. (Chapman and Hall, London, 1995).

[2] P.R.N Childs, *Practical Temperature Measurement*. (Butterworth-Heinemann, Oxford, 2001).

[3] L. Michalski, *Temperature Measurement*, 2nd ed. (Wiley, New York, 2001).

[4] A.L. Window, *Strain Gauge Technology* (Elsevier Science Publishers Ltd, Essex, 1992).

[5] R.B. Bently, in *Handbook of Temperature Measurement* (Springer-Verlag, Singapore, 1998), Vol. 2.

[6] T.D. McGee, *Principles and Methods of Temperature Measurement*. (John Wiley & Sons, New York, 1988).

[7] National Semiconductor Corporation, *Linear Databook 2*. (Globe Press, Australia, 1988), pp. 6:12-6:20.

[8] J. Turner and M. Hill, *Instrumentation for Engineers and Scientists*. (Oxford University Press, New York, 1999).

[9] Y.O. Barmenkov, C. Sifuentes, A.N. Starodumov and V.N. Fillippov, 'Fiber-optic temperature sensor based on CdSe semiconductor nanocrystal doped glass', 14th International Conference on Optical Fiber Sensors, Proc. SPIE **4185**, 78-81, (2000).

[10] M.C. Farries, M.E. Fermann, R.I. Lamming, S.B. Poole and D.N. Payne, 'Distributed temperature sensor using Nd^{3+}-doped optical fiber', Electron. Lett. **22**, 418-419 (1986).

[11] R. Hypszer, J. Plucinski and H.J. Wierzba, 'Optical fibre temperature sensor based on blackbody radiation', presented at the Optical Fibres and their Applications V, Proc. SPIE **1085**, 476-479, (1990).

[12] M. Niklès, L. Thévenaz and P.A. Robert, 'Simple distributed temperature sensor based on brillouin gain spectrum analysis', 10th Optical Fiber Sensors Conference, Proc. SPIE **2360**, 138-141, (1994).

[13] X. Bao, D.J. Webb and D.A. Jackson, '32-km distributed temperature sensor based on Brillouin loss in an optical fiber', Opt. Lett. **18**, 1561-1563 (1993).

[14] S. Trpkovski, S.A. Wade, D.J. Kitcher, G.W. Baxter, S.F. Collins, B. Dussardier and G. Monnom, 2004. 'Ultra stable fibre Bragg gratings at very high temperatures', Proc. 29th Australian Conference on Optical Fibre Technology, CD-ROM: 'ACOFT/AOS '04' ISBN 0-7315-5222-9 (ANU, ACT Australia, 2004), PO9.

[15] A.D. Kersey, M.A. Davis, H.J. Patrick, M. LeBlanc, K.P. Koo, C.G. Askins, M.A. Putnam and E.J. Friebele, 'Fiber Grating Sensors', J. Light. Tech. **15**, 1442-1463 (1997).

[16] M.G. Xu, L. Reekie, Y.T. Chow and J.P. Dakin, 'Optical in-fibre grating high pressure sensor', Electron. Lett. **29**, 398-399 (1993).

[17] S.A. Wade, S.F. Collins and G.W. Baxter, 'Fluorescence intensity ratio technique for optical fiber point temperature sensing', J. App. Phys. **94**, 4743-4756 (2003).

[18] J. Castrellon, G. Paez and M. Strojnik, 'Remote temperature sensor employing erbium-doped silica fiber', Infrared Phys. & Technol., **43**, 219-222 (2002).

[19] S.A. Wade, S.F. Collins, K.T.V. Grattan and G.W. Baxter, 'Strain-independent temperature measurement by use of a fluorescence intensity ratio technique in optical fiber', App. Opt. **39**, 3050-3052 (2000).

[20] T. Sun, Z.Y. Zhang and K.T.V. Grattan, 'Erbium/ytterbium fluorescence based fiber optic temperature sensor system', Rev. Sci. Instrum. **71**, 4017-4022 (2000).

[21] E. De La Ross, L.A. Zenteno, A.N. Starodumov and D. Mozon, 'All-fiber absolute temperature sensor using an unbalanced Sagnac loop', Opt. Lett. **22**, 481-483 (1997).

[22] T. Musher, J. Kamimura and M. Nakazawa, 'Optical phase fluctuations thermally induced in a single-mode optical fiber', App. Opt. **21**, 694-698 (1982).

[23] H-S. Choi, H.F. Taylor and C.E. Lee, 'High-performanace fiber-optic temperature sensor using low-coherence interferometry', Opt. Lett. **22**, 1814-1816 (1997).

[24] Y. Chen and H.F. Taylor, 'Multiplexed fiber Fabry-Perot temperature sensor system using white-light interferometry', Opt. Lett. **27**, 903-905 (2002).

[25] H.H. Kee, G.P. Lees and T.P. Newson, '1.65 μm Raman-based distributed temperature sensor', Electron. Lett. **35**, 1869-1871 (1999).

[26] S.F. Collins, G.W. Baxter, S.A. Wade and P.M. Farrell, 'Strain dependence of fluorescence from rare-earth-doped optical fibres: application to simultaneous, co-located, measurement of strain and temperature', Composite Struct. **28**, 373-379 (2002).

[27] M. DeMarchant, A. Brown, X. Bao and T. Bremmer, 'Structural monitoring by use of a Brillouin distributed sensor', App. Opt. **38**, 2755-2759 (1999).

[28] T. Allsop, K. Sudgen, I. Bennion, R. Neal and A. Malvern, 'A high resolution fiber Bragg grating resonator strain sensing system', Fiber and Integrated Optics **21**, 205-217 (2002).

[29] L. Yuan, L. Zhou, W. Jin and C.C Chan, 'Recent progress of white light interferometric fibreoptic strain sensing techniques', Rev. Sci. Instrum. **71**, 4648-4654 (2000).

[30] V. Lecoeuche, D.J. Webb, C.N. Pannell and D.A. Jackson, '25 km Brillouin based single-ended distributed fibre sensor for threshold detection of temperature or strain', Opt. Commun. **168**, 95-122 (1999).

[31] D.I. Forsyth, S.A. Wade, T. Sun, X.Chen and K.T.V. Grattan, 'Dual temperature and strain measurement with the combined fluorescence lifetime and Bragg wavelength shift approach in doped optical fiber', App. Opt. **41**, 6585-6592 (2002).

[32] S. Trpkovski, S.A. Wade, G.W. Baxter and S.F. Collins, 'Dual temperature and strain sensor using a combined fibre Bragg grating and fluorescence intensity ratio technique in Er^{3+}-doped fiber', Rev. Sci. Instrum. **74**, 2880-2885 (2003).

[33] C.C. Lee, P.W. Chiang and S. Chi, 'Utilization of a dispersion-shifted fiber for simultaneous measurement of distributed strain and temperature through Brillouin frequency shift', IEEE Photon. Technol. Lett. **13**, 1094-1096 (2001).

[34] S.W. James, M.L. Dockney and R.P. Tatam, 'Simultaneous independent temperature and strain measurement using in-fiber Bragg grating sensors', Electron. Lett. **32**, 1133-1134 (1996).

[35] P. W France and M.G. Drexhage [*et al.*], *Fluoride Glass Optical Fibres.* (Blackie, Glasgow UK; CRC Press, Boca Raton, Fl USA., 1990).

[36] W. Koechner, *Solid State Laser Engineering* , 4th ed. (Springer, Berlin and New York, 1995), pp. 35-36.

[37] W.J. Miniscalco, in *Rare-earth-doped Fiber Lasers and Amplifiers*, 2nd ed., edited by M.J.F. Digonnett (Marcel Dekker, New York, 2001), pp. 17-112.

[38] G.H. Dieke, 'The doubly and triply ionized rare earths', App. Opt. **2**, 675-690 (1963).

[39] B. J. Ainslie, S.P. Craig and S.T. Davey, 'The absorption and fluorescence spectra of rare earth ions in silica-based monomode fiber', J. Lightwave Technol. **6**, 287-293 (1988).

[40] M.R. Percival, M.W. Phillips, D.C. Hanna and A.C. Tropper, 'characterization of spontaneous and stimulated emission from praseodymium (Pr^{3+}) ions doped into a silica-based monomode optical fiber', IEEE J. Quant. Electron. **25**, 2119-2123 (1989).

[41] J.Y. Allain, M. Monerie and H. Poignant, 'Tunable cw lasing around 610, 635, 695, 885 and 910 nm in prasedymium-doped fluorozirconate fibre', Electron. Lett. **27**, 189-191 (1991).

[42] Y. Ohishi, T. Kanamori, T. Kitagawa and S. Takahashi, 'Pr^{3+}-doped fluoride fiber amplifier operating at 1.31 μm.', Opt. Lett. **16**, 1747-1749 (1991).

[43] Y. Nishida, M. Yamada, T. Kanamori, K. Kobayashi, J. Temmyo, S. Sudo and Y. Ohishi, 'Development of an efficient praseodymium-doped fiber amplifier', IEEE J. Quant. Electron. **34**, 1332-1339 (1998).

[44] L. Hai-Han, 'Hybrid AM-VSB/256-QAMWDM system over 70 km of single-mode fiber with praseodymium-doped fiber amplifier', Opt. Eng. **41**, 928-929 (2002).

[45] M.A. Newhouse, R.F. Bartholomew, B.G. Aitken, L.J. Button and N.F. Borrelli, 'Pr-doped mixed-halide glasses for 1.3 μm amplification', J. Non-crystalline Solids **184**, 229-233 (1994).

[46] B. Dussardier, D.W. Hewak, B.N. Samson, H.J. Tate, J. Wang and D.N. Payne, 'Pr^{3+}-doped Cs:Ga:S:Cl glass for efficient 1.3 μm optical fibre amplifier', Electron. Lett. **31**, 206-208 (1995).

[47] S.Q. Man, E.Y.B. Pun and P.S. Chung, 'Tellurite glasses for 1.3 μm optical amplifiers', Opt. Commun. **168**, 95-122 (1999).

[48] B.P. Petreski, M.M. Murphy, S.F. Collins and D.J. Booth, 'Amplification in Pr^{3+}-doped fluorozirconate optical fibre at 632.8 nm', Electron. Lett. **29**, 1421-1423 (1993).

[49] T.B. Nguyen, S. Trpkovski, P.M. Farrell, G.W. Baxter and S.F. Collins, 'Dependence of the fluorescence lifetime on dopant

concentration and temperature in praseodymium-doped fluoride glass', Opt. Commun. **186**, 277-281 (2000).

[50] Luxtron Corp., *Fluoroptic thermometers 700 series*. (Santa Clara, California, USA).

[51] L.A. Riseberg and H.W. Moos, 'Multiphonon orbit-lattice relaxation of excited states of rare-earth ions in crystals', Phys. Rev. B **174**, 429-438 (1968).

[52] C.B. Layne, W.H. Lowermilk and M.J. Weber, 'Multiphonon relaxation of rare-earth ions in oxide glasses', Phys. Rev. B **16**, 10-20 (1977).

[53] R. Reisfeld and C.K. Joergensen, *Excited State Phenomena in Vitreous Materials*. (Elsevier, Amsterdam, 1987), pp.1-90.

[54] Z.Y. Zhang, K.T.V. Grattan and A.W. Palmer, 'Thermal characteristics of alexandrite fluorescence decay at high temperatures, induced by a visible diode emission', J. App. Phys. **73**, 3493-3498 (1993).

[55] S.F. Collins, G.W. Baxter, S.A. Wade, T. Sun, K.T.V. Grattan, Z.Y. Zhang and A.W. Palmer, 'Comparison of fluorescence-based temperature sensor schemes: theoretical analysis and experimental validation', J. App. Phys. **84**, 4649-4654 (1998).

[56] V.C. Vella, T.B. Nguyen, G.W. Baxter, S.F. Collins, P.J. Newman and D.R. MacFarlane, 'Predictions of temperature independence in fluorescence lifetime of praseodymium-doped fluoride glass', Proc. 29th Australian Conference on Optical Fibre Technology, CD-ROM: 'ACOFT/AOS '04' ISBN 0-7315-5222-9 (ANU, ACT Australia, 2004) , PO4

[57] T.Sun, Z.Y. Zhang, K.T.V. Grattan and A.W. Palmer, 'Intrinsic doped fluorescence decay-time based measurements-strain and temperature characteristics for sensor purposes', Rev. Sci. Instrum. **69**, 4186-4190 (1998).

[58] Th. Tröster, T. Gregorian and W.B. Holzapfel, 'Energy levels of Nd^{3+} and Pr^{3+} in RCl_3 under pressure', Phys. Rev. B **48**, 2960-2967 (1993).

[59] P.M. Farrell, S.A. Wade, G.W. Baxter, S.F. Collins, A.J. Stevenson and K.T.V. Grattan, 'On the physical origin of strain sensitivity in optical fibre rare earth fluorescence sensors', 11th Conf. on Sensors and their Application, (IOP Bristol UK, 2001) pp. 231-236.

[60] O. Svelto, *Interaction of radiation with atoms and ions*, in *Principles of lasers*, Editor D.C. Hanna, (Plenum Press, New York USA, 1998), pp. 17-78.

[61] S.F. Collins, P.M. Farrell, S.A. Wade, G.W. Baxter, D.A. Simpson, A.J. Stevenson and K.T.V. Grattan, 'Modelling strain dependence of fluorescence from doped optical fibres: application to neodymium' Technical Digest of 15th International Optical Fiber Sensors Conference, (IEEE, Piscataway NJ USA, 2002), pp. 439-442.

[62] K.R. German and A. Kiel, 'Radiative and non-radiative transitions of Pr^{3+} in trichloride and tribromide hosts', Phys. Rev. B **11** 2436-2442 (1975).

[63] J.L. Adam, W.A. Sibley, and D.R. Gabbe, 'Optical absorption and emission of $LiYF_4$', J. Luminescence **33**, 391-407 (1985).

[64] A. Kiel and K.R. German, 'Identification of energy levels of Pr^{3+} in $LaCl_3$', Phys. Rev. B **8**, 2353-2357 (1973).

[65] Y. Shi, J.P. Ragey and O. Poulsen, 'Dye laser pumped Pr^{3+}-doped fibre lasers: basic parameter investigation, cw operation, and Q-switched operation', IEEE J. Quant. Electron. **29**, 1402-1406 (1993).

[66] M. Eyal, E. Greenberg, R. Reisfeld and N. Spector, 'Spectroscopy of praseodymium(III) in zirconium fluoride glass', Chem. Phys. Lett. **117**, 108-114 (1985).

[67] D.S. Funk and J.G. Eden, in *Rare-earth-doped Fiber Lasers and Amplifiers*, edited by M.J.F. Digonnett (Marcel Dekker, New York USA, 2001), pp. 171-242.

[68] S.A. Wade, 'Temperature measurement using rare earth doped fibre fluorescence', PhD thesis, Victoria University, 1999.

[69] J.C. Palais, *Fiber Optic Communications*, 4th ed. (Prentice Hall, Englewood Cliffs NJ USA, 1998).

[70] T.Sun, Z.Y. Zhang, K.T.V. Grattan and A.W. Palmer, 'Ytterbium-based fluorescence decay time fiber optic temperature sensor systems', Rev. Sci. Instrum. **69**, 4179-4185 (1998).

[71] S.A. Wade, D.I. Forsyth, K.T.V. Grattan and Q. Guofu, 'Fiber optic sensor for dual measurement of temperature and strain using a combined fluorescence lifetime decay and fiber Bragg grating technique', Rev. Sci. Instrum. **72**, 3186-3190 (2001)

[72] G. Laufer, *Introduction to Optics and Lasers in Engineering* (Cambridge University Press, Cambridge, 1996).

Conference papers

Koziol B.G., Collins S.F., Wade S.A. and Baxter G.W., 2004. "Temperature and strain dependence of fluorescence lifetime in Pr-doped fibres", Proc. 29th Australian Conference on Optical Fibre Technology, Canberra, CD-ROM: "ACOFT/AOS 2004" ISBN 0-7315-5222-9 (ANU, ACT Australia), PO6.

Koziol B.G., Collins S.F., Wade S.A. and Baxter G.W., 2003. "Fluorescence lifetime dependence of temperature and strain in praseodymium-doped optical fibre", Australasian Conference on Optics, Lasers and Spectroscopy 2003, Melbourne, Abstracts 265.